Determining the Cellular Targets and Resulting Pathology of Rift Valley Fever Virus Infection of the Rat CNS and Reproductive System Using Microscopy

by

Devin Alline Boyles

BS, University of Pittsburgh, 2014

Submitted to the Graduate Faculty of the

Department of Environmental and Occupational Health

Graduate School of Public Health in partial fulfillment

of the requirements for the degree of

Master of Science

University of Pittsburgh

2019

UNIVERSITY OF PITTSBURGH

GRADUATE SCHOOL OF PUBLIC HEALTH

This thesis was presented

by

Devin Alline Boyles

It was defended on

November 4, 2019

and approved by

Aaron Barchowsky, PhD
Professor
Department of Environmental and Occupational Health
Graduate School of Public Health
University of Pittsburgh

Berthony Deslouches, MD, PhD
Assistant Professor
Department of Environmental and Occupational Health
Graduate School of Public Health
University of Pittsburgh

Thesis Director: Amy L. Hartman, PhD
Assistant Professor
Department of Infectious Diseases and Microbiology
Graduate School of Public Health
University of Pittsburgh

Amy L. Hartman, PhD

Determining the Cellular Targets and Resulting Pathology of Rift Valley Fever Virus Infection of the Rat CNS and Reproductive System Using Microscopy

Devin A. Boyles, MS

University of Pittsburgh, 2019

Abstract

Rift Valley fever virus is an emerging zoonotic pathogen that infects domestic ruminants and causes fatal hepatic necrosis and "abortion storms" that result in loss of up to 90-100% of pregnancies in animals. Human infection occurs among individuals in contact with affected animals and typically manifests as a febrile illness that can advance to hemorrhagic fever or neurological disease. In patients that develop encephalitis, there is a 50% chance of death while survivors experience long-term complications. Human cases of vertical transmission during pregnancy resulted in fetal viremia, abnormalities, and death; however, the rates of congenital RVFV are misunderstood and understudied. Rodent encephalitic and congenital models of RVF have recently been developed and are crucial for elucidating the mechanism of infection separating febrile illness from severe outcomes effecting the central nervous and reproductive systems. Whole, homogenized tissues from these models have been analyzed for viral titers, infiltrating immune cells, and resulting pathologies; however, specific infection events occurring within precise tissue structures required immunofluorescence and chromogen staining for microscopic image analysis and scoring. Thin sections of tissues from both models were stained for viral and cellular markers and imaged in order to determine specific disease events observed in our lab's previous studies, Albe et al. (2019) and McMillen et al. (2018). Immunofluorescence micrographs

supported the presence of vRNA and inflammatory leukocyte infiltration in the olfactory bulbs and cortexes as early as 1 day post-infection (dpi), and massive neuronal infection and necrosis beginning by 3 dpi. End-stage neurological disease, beginning at 5 dpi, was represented by a massive blood brain barrier breakdown event and influx of inflammatory cells. Histological analysis of pregnant RVFV-infected rat tissues showed the highest amount of vRNA in the placental tissues rather than the liver, and moderate levels of virus in the uterus and ovaries. Within the placenta, RVFV targeted the maternal decidual layer and fetal basal and labyrinth zones. Viral signal was also detected in the placentas of dams that survived infection. Visual immunohistochemistry data, as developed and presented here, can help highlight structural and cellular targets of RVFV that should be focused on for therapeutic efforts. RVFV is in the Federal Select Agent program for pathogens that have the potential to post a severe threat to public, animal, or plant health, on the World Health Organization's list of Blueprint priority diseases requiring an urgent need for accelerated research and development, and a category A high-priority pathogen of the National Institute of Allergy and Infectious Diseases, which are biological agents that post the highest risk to national security; therefore research into therapeutics for RVF is of major public health significance.

Table of Contents

List of Figures

Acknowledgments

I met Dr. Amy Hartman two years ago while helping a technician in her lab learn how to stain samples for RVFV – an endeavor that still eludes me. I'm endlessly appreciative that Dr. Hartman gave me the opportunity to, not only, conduct my MS research in her lab, but also become her full-time technician. I've been fascinated by infectious diseases and virology since high school and consider the past two years working with BSL-3 pathogens the most amazing experience (and, definitely, a popular talking point for my parents to brag about). Amy has been a wonderful advisor who has helped me develop critical thinking skills and has always been supportive of my research ideas. Dr. Cynthia McMillen has also been an influential figure during my MS research; she is my mentor (who chewed my writing to bits – I actually really appreciate this), my 2am placental dissecting partner, and, most importantly, one of my best friends. My runs-ins with unsuccessful science have been made far more tolerable by her presence and inspirational quotes. I want to acknowledge Joe Albe, my fellow technician and master of all things encephalitic RVF, who has helped me every step of the way with learning virology techniques and spearheading new, innovative experiments. I wouldn't have an AIM 1 without you! Stacey, Jen, Kathi, Mike, Theron, Matt, Emily, and Henry, thank you for welcoming me to the department and helping me coordinate everything I've ever needed done during my time here. My advisor, Dr. Aaron Barchowsky for welcoming me to EOH and helping me obtain all my graduate school goals. I would also like to thank Dr. Berthony Deslouches for offering to be a part of my thesis committee. My mother who has been my number 1 fan and person who gets all my frantic phone calls, I love you. My father who genuinely enjoys hearing about my research. My fiancé, Jarod, for being my best, best friend,

1.0 Introduction

Rift Valley fever virus (RVFV) is a zoonotic pathogen of the Phenuiviridae family (previously Bunyaviridae) and *Phlebovirus* genus. This family consists of enveloped, negative-sense, single-stranded RNA viruses containing a tri-segmented genome; the individual segments are denoted as small (S), medium (M), and large (L). The genome of RVFV is highly conserved (1), approximately 11.9 kilobases long, and encodes six proteins. The S segment is ambisense and contains a non-structural protein (NSs) and the nucleoprotein (NP). The M segment contains the Gc and Gn glycoproteins and another non-structural protein (NSm). The L segment contains the RNA-dependent RNA polymerase. NSs is the major virulence factor of RVFV and acts as an antiviral immune response antagonist (2).

RVFV is endemic to the African continent and commonly infects ruminant livestock such as sheep, cattle, goat, and camels via mosquito bite of the *Aedes* and *Culex* species (3-6). Infected animals may develop fatal hepatic necrosis or experience "abortion storm" events which may cause up to 100% neonatal mortality within a herd (7). Adult animals experience a 10-20% mortality rate. Humans may contract Rift Valley fever (RVF) via mosquito bite or respiratory exposure to aerosolized virus from infected animal tissues. Individuals will typically experience a self-limiting febrile illness that can progress to hepatitis, ocular disease, and encephalitis in 1-2% of cases. Human mortality rate likely suffers from underreporting but is currently estimated to be at around 1% of cases (1). Aerosol exposure increases the likelihood of complications such as encephalitis which constitutes over a 50% mortality rate (8); farmers, veterinarians, and butchers are high risk populations for this outcome.

RVFV is on the list of Federal Select Agents and Toxins due to its potential to "pose a severe threat to public, animal or plant health or to animal or plant products" (9). The World Health Organization (WHO) also considers RVF to be a public health concern and has it on the Blueprint list of Priority diseases for accelerated therapeutic research and development efforts. The current vaccines for livestock are either ineffective or teratogenic and, currently, there are no therapeutics to treat severe disease among humans. While outbreaks have only occurred on the African continent, Arabian Peninsula, and Madagascar, the mosquito species that are competent to transmit RVFV also inhabit North America and Europe. Other mosquito-borne viruses, Chikungunya virus (CHIKV) and West Nile virus (WNV), can serve as examples of imported pathogens that were able to successfully find reservoirs in the Americas (10). The potential for RVFV to spread to naïve populations is of major concern for human and animal health due to the ability to cause severe disease and economic burden.

1.1 Rift Valley Fever Virus

1.1.1 Epidemiology and Transmission

The first recorded animal outbreak of RVFV occurred in the Rift Valley of Kenya in 1931. The British Division of Veterinary Research investigated an abrupt and severe illness among lambs which resulted in death 24-hours after initial symptom onset (11). Severity of disease was age-dependent with mortality rates near 95% among 3-7-day old lambs. Abortion storms occurred among asymptomatic pregnant ewes, while non-pregnant adult sheep experienced lethargy, vomiting, and diarrhea (12). Postmortem examination of the infected animals showed extensive

liver necrosis (12). It is likely that RVF epizootic outbreaks occurred before 1931 since high-mortality miscarriage events among livestock were noted previously. RVF epidemics have since spanned many regions of Africa such as Kenya (12-14), Egypt (14, 15), Sudan (16), Tanzania (14, 17), Mauritania (18, 19), and the Middle East (8). In 2000, the first recorded outbreaks outside of Africa occurred in the Saudi Peninsula, Yemen (2), and Madagascar (20). Recent outbreaks in Gambia and South Sudan in 2018 highlight the continued prevalence of this disease in Africa and the Middle East (14).

Scientists and veterinarians involved in the 1931 Rift Valley outbreak investigation were the first humans to test seropositive for RVF. Samples from farmers of infected herds were retroactively tested and also found to have RVFV-specific neutralizing antibodies (12). Disease was reproduced in another human subject via needle injection with blood from an infected lamb. The patient developed a "dengue-like" illness including "fever, headache, abdominal pains, joint and muscle pains, photophobia, retro-orbital pain, vomiting, nosebleeds, and sweating." (12).

Human epidemics highlight the increased incidence of RVF in populations that raise and cohabitate with livestock. In 1977, Egypt experienced the deadliest outbreak to date with 200,000 infections and 600 deaths (15); strain ZH501 was collected and purified from this outbreak and is currently used as one of the most pathogenic laboratory strains. A more recent outbreak in 2007 that occurred in Sudan had 747 confirmed cases of RVF and 230 deaths; although the total number of cases is thought to be closer to 75,000 and underreported due to lack of medical infrastructure and the similarity of RVF symptoms to other diseases (16).

RVF outbreaks occur during times of heavy rainfall and flooding which promote breeding of mosquito species in the *Culicidae* family. The major mechanism of persistence during inter-epidemic periods is transovarial transmission from mosquitos to offspring, bloodmeal infection of

livestock or wild ruminants, and infected livestock infecting naïve mosquitos (21). Field seroprevalence investigations show that RVFV can infect a wide range of wild ruminants such as buffalo (22), waterbuck (22), impala (22, 23), and kudu (22) and non-ruminants such as warthogs and domesticated pigs (24). There are similar American species such as pronghorn, elk, and deer that could act as a reservoir in the event of RVFV spreading to the United States (US) (21). White-tailed deer are widely distributed across the US with territories overlapping with humans. They are a common source of bloodmeals for mosquitoes and are reservoirs for other bunyaviruses such as La Crosse virus (LACV), Jamestown Canyon virus (JCV), and Cache Valley virus (25). Five-month-old male white-tailed deer were subcutaneously injected with wildtype (WT) RVFV (Kenya 2006 strain) and developed high viral titers at 2 days post-infection (dpi) (26). Two of the five deer developed bloody diarrhea and died by 3 dpi. Severe hepatic necrosis and enteritis were found in the two deer with diarrhea during necropsy. The uninfected control deer developed RVF symptoms shortly after exposure to bloody diarrhea which suggests horizontal transmission from infected feces. Cell lines of other US species such as pigs, dogs, cats, coyotes, and frogs (21) were permissive to RVFV infection. This suggests that RVFV introduction into the US could have critical effects on wildlife and domesticated animals.

The lack of vaccines and therapeutics towards RVFV infection and its ability to cause severe disease via inhalation requires it to be studied under biosafety level 3 (BSL-3) containment requirements. Researchers must don positive air pressure respirators and work in negative pressure laboratory spaces. At least 25 accidental lab-acquired infections occurred through 1949 (27, 28) with a total of 47 to date. These incidents were mostly caused by aerosol exposure.

1.1.2 Viral Replication

Glycoproteins, Gn and Gc, aid in host cell attachment, entry, replication and release of RVFV by recruiting the viral RNA-dependent RNA polymerase to the golgi apparatus and packing of viral NP (29). RVFV enters host cells using caveolin-1-mediated endocytosis with DC-SIGN (found on dendritic cells and macrophages) and heparan sulfate (expressed by most cell types) as mediating cell surface markers (29-31). Viral replication occurs in the cytoplasm with one cycle lasting about 10-12 hours (32). The nonstructural proteins of RVFV can hijack the immune system. NSm delays virus-induced apoptosis which allows for infected cells to evade death and spread virus (33, 34). NSs inhibits interferon (IFN) production by blocking transcription of the interferon-beta (IFN-B) promoter and transcription factor II H (TFIIH) (34); this mechanism prevents induction of antiviral genes in infected cells (32, 35). NSs also inhibits host RNA polymerase II which prevents successful synthesis of IFN mRNAs (36). Gn, Gc, and NP are the common antigenic proteins and are targets of therapeutics currently in development but have yet to gain U.S. Food and Drug Administration (FDA) approval.

1.1.3 Pathogenesis and Disease in Humans

RVFV has an incubation period of about 4-6 days. Initial flu-like symptoms start abruptly, namely: chills, malaise, dizziness, weakness, headache, and nausea. Fever resulting in an elevated body temperature between 38.8 °C and 39.5 °C is accompanied by decreased blood pressure, body pains, rigor, shivering, red or sore eyes, constipation, insomnia, and photophobia (37). Epistaxis, abdominal pain, vomiting, and diarrhea can occasionally develop. Fevers typically dissipate within three days and body temperature will return to normal. RVF may result in a biphasic fever 1-3

days after initial fever recovery that can last up to ten days (38). About 1% of RVF cases result in mortality; death typically occurs 3-6 days after severe symptom onset (1). These patients typically have elevated liver enzymes, aspartate transaminase (AST) and alanine transaminase (ALT), and decreased platelets. Liver hemorrhage is the most common cause of death, though, there are few cases where renal failure and thrombosis were present in the absence of liver pathology.

Neurological disease develops in about 1-2% of severe RVF cases and is characterized by symptoms such as ataxic gate, retinal hemorrhage, meningeal irritation, confusion, coma, hyper-salivation, teeth-grinding, and visual hallucinations (37). Pathological observation into tissue samples from patients with neurological disease show brain lesions with neuronal necrosis, immune cell infiltration and perivascular cuffing (37). Ocular disease may develop alongside neurological symptoms and will resolve itself in about 50% of cases, however, if RVFV causes lesions to develop in the macula or retina of the eye patients may experience permanent vision loss (8, 39, 40).

Human vertical transmission of RVFV is understudied and likely underreported, however, the high rates of fetal abortions among livestock make this source of infection one of concern. There are two case studies showing evidence of congenital RVF in humans. A pregnant Sudanese woman with RVF symptoms and RVFV-specific IgM delivered a child with RVFV-specific IgM exhibiting skin rash, enlarged spleen and liver, and jaundice (41). Another pregnant woman with an ongoing RVF infection gave birth to an infant who died within a week from the disease (42). A cross-sectional study of 130 pregnant Sudanese women showed higher rates of second and third-trimester miscarriages in individuals with confirmed RVF infection (43).

McMillen et al. (2018) infected human placental explants with RVFV to evaluate tissue permissivity. RVFV efficiently replicated within the chorionic villi and outer syncytial layers;

these tissues exhibited a 2-3 log increase in virus production between 12-36 hours post-infection (hpi) (44). RVFV targeted the villus structure and syncytiotrophoblast cells which can resist many other viruses, such as Zika virus (ZIKV) (45). Pregnant rats, often used in human placental development and toxicology studies, were also found to transmit RVFV to their offspring *in utero* (44) similar to what is observed in livestock and humans.

1.1.4 Prevention and Treatment

The most promising preventative method for RVF infection and disease in livestock is prophylactic vaccination. The first live-attenuated vaccine for livestock was developed in the 1960's and was found to be teratogenic in pregnant ruminants. There are no vaccines or antiviral treatment options available for RVFV infection in humans (46, 47); supportive care is the only option to treat severe disease outcomes such as hemorrhagic fever or neurological disease (14). Due to the ability of RVF infection to result in hepatic, hemorrhagic, neurological, or ocular disease, there is a critical need for therapeutics that target each unique outcome.

Smithburn, the first vaccine strain, was developed by serial passaging virulent RVFV in a mouse brain (48). Vaccination with this strain caused abortions and had teratogenic effects in livestock, therefore it was only used for non-pregnant animals during severe outbreaks. A formalin-inactivated version was produced but had decreased efficacy and required boosters. A cause for concern with bunyaviruses is their ability to reassort with others within the order (49); reassortment with virulent strains is a risk for all attenuated vaccines (50).

The United States Army Medical Research Institute of Infectious Diseases (USAMRIID) developed an attenuated vaccine strain of RVFV, MP-12, in response to the devastating 1977 outbreak in Egypt. Virulent ZH548 was passaged in the presence of 5-fluorouracil to induce

mutagenesis in all three RNA segments (51, 52). MP-12 is licensed and approved for veterinary use in the United States and is safe and efficacious in non-pregnant animals (53). A vaccine trial in sheep showed that MP-12 also induced abortions and teratogenesis during early pregnancy. However, MP-12 is currently in a phase II clinical trial for human prophylactic use (54); studies evaluating vaccine safety for pregnant individuals will need to be carried out.

Another vaccine strain of RVFV, Clone 13, contains a deletion in the NSs coding region (55); due to this large deletion, it is highly unlikely that this strain can revert to WT without reassortment with a pathogenic strain. Immunization with this strain was found to stimulate strong antibody responses and did not cause abortions or teratogenesis. This vaccine is not FDA approved but is utilized for livestock in places experiencing outbreaks (56).

Palliative care is the only means of treatment for RVF (38). Nucleoside analogs, such as ribavirin and favipiravir, have been investigated for antiviral use. Ribavarin was approved for treatment of RNA virus diseases such as Bolivian hemorrhagic fever (BHF), Lassa fever, and Argentine hemorrhagic fever (AHF) (57, 58). Ribavarin was also used in a mouse model of Punta Toro virus (*phlebovirus*) infection. It significantly impaired viral replication and resulted in 100% survival in animals given subcutaneous (SUBQ) (59) or intraperitoneal (IP) (60, 61) challenge with daily SUBQ administration. However, aerosol-challenged mice were not protected (62). Side effects such as inflammation and hemolytic anemia can develop from use of ribavirin (63). Favipiravir is a polymerase inhibitor that is currently approved for use in influenza-infected patients in Japan. It had also been found to be efficacious as a broad-spectrum antiviral against various RNA viruses in the filo-, aerna-, paramyxo-, and bunyavirus orders (59, 64-68). *In vitro* studies show promising antiviral effects against bunyaviruses, including RVFV, by protecting against acute hepatic infection (64). In a RVFV hamster model, favipiravir given twice orally for

10 days protected 80% of the infected animals (59). Favipiravir cannot easily cross the blood brain barrier (BBB) and would not be successful as an antiviral for neurological RVF (59, 69).

Virus-like particles (VLP) against RVFV may bridge the gap between the development of efficacious immunogenic therapies without pathogenic viral reversion or health side effects. VLP-based vaccines do not contain viral genetic material and can be made using baculoviruses (rBV) expressing RVFV Gn, Gc, and NP proteins (70). RVFV VLPs induced high virus-neutralizing antibody titers in mice given three immunizations and eleven out of twelve mice survived infection (71). RVF virus replicon particle (VRP$_{RVF}$) vaccines have also been efficacious in mouse models at only a single dose (72). This agent can actively synthesize RVFV viral RNA (vRNA) and proteins but lacks glycoprotein genes, because of this, there is a low chance of reverting to virulence (72). It was found safe for intracranial inoculation of suckling mice and completely protected against 100,000 times the median lethal dose (LD$_{50}$). The RVFV VLP and VRP$_{RVF}$ vaccines induced a systemic antiviral and adaptive immune response without the risk of pathogenic reversion and should be further explored as treatments.

1.1.5 Public Health Significance

RVFV is listed as a category A high-priority pathogen by the National Institute of Allergy and Infectious Diseases (NIAID) and a select agent by the United States Department of Health and Human Services (DHHS) and Department of Agriculture (USDA) due to its potential for introduction into the country, intentionally or accidentally, and its ability to cause severe disease in naïve populations for which there are no approved therapeutics. The Centers for Disease Control (CDC), NIAID, and the USDA deem RVFV a select agent because of its capability to be used as a bioterrorism agent if aerosolized. Research by the United States and Russia during the Cold War

found that aerosolized RVFV was stable (with a half-life of 77 minutes at room temperature and 30% relative humidity) and could successfully spread via inhalation (73). The WHO modeled the ability of RVFV to spread in the event of a bioterrorism attack and determined that if an aircraft released 50 kilograms of virus over a population of 500,000 individuals that an estimated 35,000 people would be incapacitated and, of those, 400 would die (74).

International travel broadens the risk for RVFV spread to naïve countries; over 97% of individuals traveling to the United States from RVFV-endemic countries typically arrive at airports in densely populated cities such as New York City, Washington DC, Atlanta, Baltimore, Newark, and Houston (75). Europe, North America, and South America have the *Aedes* and *Culex* mosquito species that can serve as vectors for disease as well as domestic and wild ruminants that can act as a reservoir (21, 26). Climate change has also increased the range of mosquito species already harboring RVFV. It has also been shown that a single infected mosquito can be sufficient for viral invasion to a naïve country (76). In the event of its spread to the United States, RVFV could have devastating consequences for humans and livestock.

The Zika virus outbreak in the Americas in 2015-2016 raised concerns over the congenital and neurological side effects of infection in pregnant women and their offspring. Of 28,000 confirmed Zika cases, about 1,000 (4%) were pregnant women (40). The two human case studies of vertical transmission of RVFV mimicked the phenomena seen in livestock and prompted the development of a rodent model of congenital infection in McMillen et al. (2018). Pregnant rat dams that survived infection gave birth to offspring with severe congenital abnormalities which emphasizes the long-term consequences of RVFV infection even in subclinical cases. These findings highlight the need to develop therapeutics for sensitive populations including pregnant women and developing fetuses.

1.2 Animal Models

1.2.1 Mice

Mice are very susceptible to RVFV infection and require an attenuated strain lacking the major virulence factor, NSs, in order to survive infection long enough for observation. Mice infected with wildtype RVFV strains (ZH501 and ZH548) will show decreased activity in 2-3 days and typically die within 24 hour of symptom onset. Death consistently occurs within 3-5 days due to fatal hepatitis regardless of dose or exposure type (77). Mice given an attenuated RVFV strain with a deletion in the NSs gene (del NSs) intranasally will develop lethal neurological disease and die within 7-9 days. Del NSs footpad injection results in subclinical disease characterized by a rapid and robust antibody response and T cell involvement (77). Mice lacking functional IFN-alpha/beta systems (IFNAR$^{-/-}$) also develop severe disease when exposed to attenuated RVFV strains such as MP-12 due to the inability to mount any IFN-based antiviral responses (78). These strains are useful for studying attenuated vaccinations containing DNA plasmid vector encoded RVFV segments and their ability to prevent disease despite the mice not having a proper antiviral response (79).

RVF pathology in the mouse model mimics what is observed in lambs, namely, an acute hepatic disease with the potential to lead to encephalitis. Hemorrhagic fever and ocular disease do not occur in any mouse strains (80). Histological analysis shows eosinophilic inclusion bodies in hepatocytes and lymphocyte apoptosis during hepatic disease and neuronal necrosis, microvascular hemorrhaging, and perivascular cuffing in neurological disease (80).

Although mouse models are invaluable for exploring the differences between immune responses between lethal and subclinical RVF in mice, the inability to use pathogenic RVFV is a major limitation.

1.2.2 Rats

RVF disease outcome in rats is dependent on the strain (56), dose, and exposure route (81). Wistar-Furth rats succumb to hepatic disease and viremia within a few days of SUBQ infection with pathogenic RVFV (56). August Copenhagan Irish (ACI) rats are only moderately susceptible to subcutaneous infection and about 50% succumb to neurological disease similar to what is observed in humans (56). Lewis rats do not develop clinical disease after SUBQ infection but become viremic and by the end of infection no virus is found in the brain, other tissues, or blood (56). The Hartman lab has developed both a reproducible immunocompetent rat model of encephalitic disease in Lewis rats and a congenital model in pregnant Sprague-Dawley rats (44, 82).

When infected with 10^3 plaque-forming units (pfu) of ZH501 via inhalation of small particle aerosols, Lewis rats will develop encephalitic disease within 5-7 days post-infection (dpi) and succumb by 6-7 dpi. Clinical symptoms manifest as fever, weight loss, ruffled fur, hunched posture, and porphyrin staining of the eyes, nose, and mouth. Neurological symptoms manifest as cage circling, horizontal rolling, head tilting, head and neck tremors, and erratic behavior such as jumping. Prior to the clinical window of disease there are alterations in leukocytes and inflammatory cytokines (82). Moderate levels of virus (10^4-10^6 pfu/g) were detected in the lung from 1-5 dpi (peaking at 3 dpi) which decreased to undetectable levels by 7 dpi; despite viral infiltration of the lung, there were no noticeable pathological changes. Liver and spleen are primary

targets of viral replication in livestock and most rodent models of RVFV, however, in the Lewis rat model, liver and spleen displayed low levels (10^2-10^3 pfu/g) of infectious virus at 3-4 dpi and had no noticeable pathological changes or elevated liver enzymes. The brain had detectable viral RNA at 1 dpi and infectious virus by 5 dpi (10^7-10^9 pfu/g) which persisted for the duration of the study (7 days). Lymphocytic meningitis, vasculitis of lymphocytes, neutrophils, and cortical neurons with apoptotic morphology were evident in the rats by 6-7 dpi. Infectious virus was also found in the eyes. Immunohistochemistry (IHC) staining showed an association between apoptotic cells and viral antigen. Cytokine dysregulation is also a feature of this model showing elevated levels of MCP-1, M-CSF, Gro/KC, RANTES, and IL-1β which peak at 4 dpi, suggesting monocyte, macrophage, and neutrophil recruitment to the CNS. Elevated levels of MCP-1, RANTES, and Gro/KC have also been seen in other viral encephalitic diseases such as tick borne encephalitic (TBE), Semlike forest virus (SFV) and WNV (83, 84).

Walters et al. (2019) found elevated levels of matrix metalloproteinase 9 (MMP-9), an enzyme that modifies BBB integrity by degrading tight junctions and extracellular matrix of vascular endothelium, in RVFV-infected Lewis rats given aerosol challenge. MMP-9 elevation is concurrent with increasing viral RNA levels towards end stage disease. Vascular imaging of infected rat brains observed a minor blood brain barrier (BBB) leakage event, occurring on 1 dpi, followed by viral RNA entry into the brain. A massive leakage event occurred 4-5 dpi right before clinical manifestation of symptoms (85). MMP-9 is also involved in WNV entry into the brain after a BBB opening event in mice (86). Vascular breakdown is also a component of infection by LACV (87).

Albe et al. (2019) observed vascular leakage, viral entry, and immune cell infiltration into the brain of rats given 10^3 pfu of pathogenic RVFV via aerosol. Lewis rat serial sacrifice

13

experiments compared aerosol and SUBQ exposure disease manifestations. An LD_{50} of 10^2 pfu was observed for aerosol exposure with 100% mortality over the 7-day infection period whereas the LD_{50} for SUBQ exposure was greater than 10^5 pfu and only resulted in about 20% mortality. A steady rise in viral RNA in the central nervous system (CNS) tissues began at 1 dpi and peaked to 10^7 pfu/g in the aerosol model; spleen and liver reached similar titers by end stage infection. In the SUBQ model, the CNS tissues only reached 10^2 pfu/g (as early as 1 dpi) but reached 10^5 pfu/g in the liver by 4 dpi. Total white blood cells (WBC) and platelets followed similar patterns until the 5-7 dpi clinical window where WBCs increased to the end of infection in aerosol exposure and slowly declined in SUBQ exposure. The aerosol model was characterized by a massive infiltration of neutrophils and leukocytes ($CD45^+$ cells) during 5-7 dpi. Cells being labeled with CD45 are characterized as: $CD45^{high}$ being infiltrating monocytes, macrophages, and activated microglia and $CD45^{med}$ being quiescent microglia (88).

A decrease in lymphocytes at 3 dpi marked the first change in blood composition followed by granulocytosis and thrombocytopenia for the duration of infection. Neutrophils are also the first immune cells to enter the brain of Lewis rats during the clinical window of encephalitic disease (82, 88). These symptoms are similar to neurological RVF in humans (8, 37, 89).

An understudied mechanism of infection for RVFV is its ability to enter the brain through the olfactory epithelium after aerosol exposure. The connection between the olfactory nerve and the CNS is short and channels formed between individual olfactory neurons can fit particles up to 100nm (90), thus bunyaviruses, which are 90 to 100 nm in diameter (90), can pass. Rats exposed to aerosolized RVFV exhibit neutrophil and monocyte influx into the brain at the beginning of the clinical window, although virus is seen as early as 1 dpi (88). Since RVFV reaches the brain by 1

dpi in both the aerosol and SUBQ route but only causes mortality in the aerosol model, investigation into viral activity in the olfactory epithelium is crucial.

McMillen et al. 2018 developed the first reproducible rodent model of congenital RVFV in Sprague-Dawley (SD) rats. Pregnant rats that were subcutaneously infected with ZH501 exhibited vertical transmission and intrauterine fetal death similar to what is seen in livestock (81). Vertical transmission occurred in both rats that succumbed to RVF and rats that survived. Sublethal rats gave birth to still-born pups with gross pathological changes such as fluid accumulation (fetal hydrops), gray discoloration, and stunted development (44). Viral titers, in this model, were higher in the placenta than the liver which challenges RVFV hepatotropic nature after SUBQ exposure (44). Rat and human placentas have morphological differences; however, they are similar enough that rats are commonly used to study placental development and vaccine teratogenicity during pregnancy (91). Both human and rat placentas are hemochorial and have maternal blood in direct contact with the chorion membrane that surrounds the embryo. There is also deep, intrauterine trophoblast cell invasion which facilitates blood exchange between maternal and fetal tissues; this gives pathogens a direct infection pathway to the fetus (92). This model of disease is poorly understudied. Utilizing a reproducible animal of congenital RVF can help elucidate the cellular targets of the virus and gestational stages in which protective therapeutics should be aimed. Studying the effects of RVFV on reproductive and fetal tissues is also crucial for mitigating negative effects in current live-attenuated vaccines.

1.2.3 Non-Human Primates

Rhesus macaques are the most commonly used non-human primate (NHP) model in RVF studies and develop a nonlethal fever after aerosol exposure. Various infection routes

(subcutaneous, intravenous, and aerosol) have resulted in viremia, non-lethal fever and, rarely, lethal hemorrhagic disease. Low viral replication was noted from serum antibody titers (93). The Hartman lab has published RVFV infection data in three other NHP species: cynomolgus macaque, African green monkeys (AGM), and marmosets in order to categorize and develop an encephalitic model more phylogenetically similar to that of humans. Cynomolgus macaques developed fever similar to rhesus macaques but did not develop neurological disease (93). Marmosets succumbed to severe neurological disease from intranasal (93, 94) and low-dose aerosol exposure; encephalitis was observed at high-dose aerosol exposure (93). Subcutaneous infection of marmosets resulted in hepatitis and hemorrhagic fever. AGMs experienced similar neurological disease when infected via aerosol with 5 out of 6 succumbing to encephalitis. Subcutaneous exposure, however, produced no symptoms or deaths. Enzyme-linked immunosorbent assay (ELISA), complete blood count (CBC), and blood chemistry analyses showed high amounts of RVFV IgG in the brain tissues, decreased platelet counts, and granulocytosis similar to that seen in the Lewis rat encephalitic model (93). This preliminary study on marmosets and AGMs has laid a foundation for the use of these models in exploring neurological RVF.

1.2.4 Other models

RVFV infection in other rodents results in unique outcomes. Syrian hamsters are very susceptible and die from liver disease 2-3 days post-infection, similarly to mice. Neutralizing antibody treatment can prevent liver necrosis, but fatal encephalitis usually develops by 11 dpi (95). Gerbils develop encephalitis with severity being age dependent. 10-week old gerbils exhibit around 50% mortality. Mortality rate increases with decreasing age (95).

2.0 Statement of Project and Specific Aims

Animal models that yield similar disease outcomes as humans are invaluable for defining the mechanism of infection for emerging pathogens such as RVFV. Newly developed rodent models of neurological and congenital RVF open new doors to elucidating therapeutics for disease of the CNS and reproductive system due to their similarity in structure and pathology to what is observed in human cases. There is a lack of understanding of how RVFV causes encephalitic and congenital disease; namely, how the virus enters these tissues, which cells become infected, and whether the pathology is primarily caused by the virus or inflammatory immune cells. Previous research into these models characterized viral and immune cell infiltration into whole tissues, however, seeing specific infection events at the cellular level is necessary to confirm the infection mechanisms of RVF disease trajectory. Based on the data presented above, *we hypothesize that early and extensive viral entry into the CNS from AERO exposure causes an inflammatory immune cascade that results in lethal encephalitic disease, accounting for the difference in mortality from that seen in SUBQ models. In the congenital rodent model, we hypothesize that RVFV is able to directly infect the maternal-fetal interface of the placenta, which is made up of immunologically-privileged cell types; the affinity of RVFV to these cell types allows for severe reproductive system pathology and miscarriages similar to what is seen in livestock, and, potentially, humans.* We will use the following specific aims to address unmet needs in visualization of RVFV infection in CNS and reproductive tissues:

Aim 1: To develop immunofluorescence staining techniques to characterize the trajectory of RVFV infection and corresponding inflammatory immune response in the nasal epithelium

and brain during RVF encephalitis in rats. The repercussions of immune cell infiltration into the central nervous system (CNS) during RVFV aerosol infection are not extensively studied. Our lab observed that the immune response to infection was at least partly responsible for uncontrolled inflammation and cytokine storms resulting in tissue pathologies in the rat model of RVF encephalitis. In vitro infections show neuronal and microglial cell types to be permissible to RVFV. *Our working hypothesis is that inhaled Rift Valley fever virus first infects the olfactory epithelial neurons and travels across the axons into the olfactory bulb of the brain. Viral infection then stimulates an influx of inflammatory immune cells that further damages the neuronal population and, ultimately, leads to the death of the animal.* Fluorescent RNA in situ hybridization (RNA ISH) of viral RNA and immunostaining of immune cell infiltrates will be used to identify inflammatory cell infiltrates and resulting pathologies of infected rat brains and snouts compared to uninfected controls.

Aim 2: To define the mechanism of RVFV infection in the placenta and reproductive tissues of pregnant Sprague-Dawley rats. Our recent work defined the first rodent model of vertical transmission of RVFV. Pregnant rats were more likely to succumb to infection than non-pregnant rats, and the virus was able to bypass the antiviral protections of the reproductive system and directly infect the placenta. Even asymptomatic mothers that survived to give birth produced stillborn pups or pups with severe abnormalities. Little is known about the mechanism of viral infection in the placenta and the resulting fetal pathology. *Our hypothesis is that RVFV infects otherwise protected reproductive structures and stimulates an inflammatory immune response that damages the fetus during gestation resulting in growth restriction and fetal death.* RNA ISH of viral RNA and immunohistochemical (IHC) staining of immune cells will be used to identify

18

inflammatory cell infiltrates and the resulting pathologies of lethally infected and sublethally infected rat maternal and fetal tissues compared to that of infected non-pregnant, pregnant uninfected, and non-pregnant uninfected controls.

Characterizing the timeline of RVFV infection and immune cell infiltrates responsible for pathogenesis in encephalitic and congenital models of RVF is crucial for elucidating targets for antiviral therapies. This work will provide preliminary insight into the cellular targets of RVFV and the host immune response and aid in determining the major cause of tissue damage during encephalitic and congenital RVFV.

3.0 Materials and Methods

3.1 Biosafety

All work with ZH501 RVFV was performed in the biosafety level 3+ Regional Biocontainment Laboratory (RBL) at the University of Pittsburgh. Personnel wore powered air purifying respirators (PAPRs), waterproof apron, and facility designated shoes. The RBL is a shower-out facility that requires a full clothing change into scrubs before entry and a personal shower and new scrubs upon exit. Work was conducted in a class III biosafety cabinet (BSC) using Vesphene IIse (Steris Corporation, cat. #646101) at a 1:128 working dilution as a disinfectant. All tissues or samples removed from BSL-3 were inactivated using methods described below; all inactivation methods have been verified and approved by a University of Pittsburgh biosafety oversight committee.

3.2 Virus and Cells

The ZH501 strain of RVFV used in these experiments was provided by Barry Miller (CDC, Fort Collins, Colorado) and Stuart Nichol (CDC, Atlanta, Georgia). Virus was propagated from VERO E6 (CRL-1586, American Type Culture Collection) cells in standard culture conditions using Dulbecco's modified Eagle's medium (DMEM) containing 2% (D2) or 10% (D10) fetal bovine serum (FBS), 1% penicillin-streptomycin (pen/strep), and 1% L-glutamine.

3.3 Rat Experiments

All animal work was conducted at animal biosafety level 3+ (ABSL-3+) conditions. Experimental plans were reviewed and approved by the University of Pittsburgh IACUC. For the encephalitic RVFV model, female Lewis rats (8-10 weeks of age) were infected with RVFV ZH501 at $3x10^4$ pfu for aerosol (AERO) exposure and $1x10^5$ pfu for subcutaneous (SUBQ) exposure. Two rats were euthanized per day from days 1-7 dpi to collect tissues. Rats meeting euthanasia criteria before 7 dpi (end of experiment) were sacrificed. Aerosol infections were performed in a class III aerobiology cabinet.

Sprague-Dawley (SD) (6 to 8 weeks of age) were inoculated in the hind flank with 500uL of RVFV ZH501 diluted with DMEM + 2% FBS. Pregnant rats were inoculated on embryonic day (E) 14 (by this time the placenta has fully formed) in four different dose groups (7.5×10^1 pfu, 1.8×10^2 pfu, 1.5×10^3 pfu, and 2.6×10^4 pfu). Dams that met euthanasia criteria were sacrificed, otherwise they were sacrificed at 18 dpi along with their surviving offspring. Nonpregnant dams were euthanized at 16 dpi unless euthanasia criteria were met beforehand.

3.4 Tissue Preparation

3.4.1 Central nervous system sample preparation for immunofluorescent *in situ* hybridization

Lewis rat tissues were perfused with 500mL of 4% paraformaldehyde (PFA) following euthanasia to ensure complete inactivation of tissues in the entire animal then then submerged in

fresh 4% PFA and stored at 4°C for fixation for at least 3 hours (brain tissue) or 1 week (whole rat head/snout) before removal from BSL-3 conditions. Tissues were cryoprotected using 30% sucrose and flash frozen with liquid nitrogen-cooled 2-methylbutane. Frozen samples were sectioned at 7µm using a microtome supplied by the University of Pittsburgh Center for Biologic Imaging.

3.4.2 Nasal turbinate tissue preparation for immunofluorescence

Heads (1 per timepoint) from the Lewis rat encephalitic model were submerged in 4% PFA after perfusion fixation for 1 week before removal from BSL-3 conditions. Due to nasal turbinate bone in the tissues, samples required a decalcification step with pH 7.4, 10% ethylenediaminetetraacetic acid (EDTA) with distilled water for three weeks; each week the sample was moved to a container of fresh EDTA; EDTA is gentle on tissues, preserves DNA, and ideal for use with immunofluorescence (96). After decalcification, the heads were washed with 1x PBS and placed in 70% ethanol for transport to the University of Pittsburgh, McGowan Institute Histology Core for paraffin embedding and sectioning of the region of the turbinate with the most olfactory epithelium surface area (T3 and T4).

3.4.3 Reproductive tissue sample preparation for chromogen in situ hybridization

Pregnant SD rat tissues were harvested without perfusion and submerged in 4% PFA for 24 hours and stored at 4°C. Samples were moved into fresh 4% PFA for removal from the BSL-3 facility. Tissues were paraffin embedded and sectioned at the University of Pittsburgh McGowan Institute Histology Core.

3.5 RNA *In Situ* Hybridization and Immunofluorescence

3.5.1 Encephalitic model immunofluorescence and in situ hybridization of brain tissues

The neurological RVFV serial sacrifice experiment contained 16 Lewis rats; two uninfected controls, and two rats per day post-infection (1 dpi through 7 dpi). All replicates (two rats per day) were stained and imaged along with a primary delete slide that did not receive the primary antibody incubation step. The primary delete internal control is used to determine if tissues express non-specific fluorescence or if the secondary antibodies bind non-specifically; images of this slide are used to set analysis parameters. Slides were stained in slide boxes lined with wet paper towels (in order to create a humidity chamber to prevent the samples from drying out) and placed in an incubator at 37°C in place of the RNAscope hybridization oven; this method was able fit more slides in one experimental run than the hybridization oven, which only holds 20 slides. Slides were permeablized for 30 minutes using 0.1% TritonX100 detergent + 1x PBS at room temperature (RT, 25°C); permeablizer was placed on the slide in enough volume to cover the tissue. TritonX100 is a strong detergent that partially lyses cell membranes which is required for viral antigen and probe staining. The protease step in the RNAscope kit was omitted to preserve microglia and neuronal antigen, which are degraded by this reagent. Slides were stained in slide boxes lined with wet paper towels and placed in an incubator at 37°C in place of the RNAscope hybridization oven. Donkey serum (20% in 5% BSA + 1x PBS), specific to the host of the secondary antibodies, was used to block non-specific binding of secondaries for 45 minutes at RT. Primary antibodies that target microglia (goat anti-IBA-1; Novus, Catalog #NB100-1028; used at 1:100 with 5% BSA + 1x PBS), neutrophils (rabbit anti-myeloperoxidase; Abcam, catalog #ab9535; used at 1:200 with 5% BSA + 1x PBS), and leukocytes (mouse, cy5 pre-conjugated

23

CD45; BD Pharmigen, catalog #565465; used at 1:100 with 5% BSA + 1x PBS), and a dye that stains neuronal Nissl bodies (647-conjugated Neurotrace; Invitrogen, catalog #N21843; used at 1:100 with 5% BSA + 1x PBS), were incubated for 1 hour at 4°C. Fluorescent secondary antibodies that target the primary antibody host species (Donkey anti-goat IgG H&L Alexa Fluor 488, Abcam, catalog #ab150129; Cy™3 AffiniPure Donkey Anti-Rabbit IgG (H+L), Jackson ImmunoResearch, catalog #711-165-152) were incubated for 1 hour at RT in order to tag primary antibodies. Hoescht (Bis-benzamide) was incubated for 1 minute to counterstain the nuclei at 450 nanometers (nm). Samples were mounted using a glycerol and polyvinyl alcohol (PVA) mixture.

3.5.2 Encephalitic model immunofluorescence of nasal epithelial tissues

Nasal turbinate slides were deparaffinized using an alcohol dehydration series (100%, 95%, and 70%; each step was repeated two times using fresh reagents and a 20-minute incubation time; increased incubation time was needed to account for size of tissue section). Slides underwent an antigen retrieval process by boiling in pH 6.0, 10mM sodium citrate buffer with 0.05% Tween-20 for 15 minutes to unmask antigen and probe-binding epitopes. Slides were permeablized for 30 minutes using 0.1% TritonX100 detergent + 1x PBS at RT; Serum specific (20% in 5% BSA + 1x PBS) to the host of the secondary antibodies (donkey) was used to block non-specific binding of secondaries for 45 minutes at RT. Primary antibodies that target olfactory epithelial neurons (sheep anti-OMP; Thermofisher, catalog #OSS00001W, used at 1:200 with 5% BSA + 1x PBS) and RVFV NP antigen (supplied by Dr. Anita McElroy, University of Pittsburgh Center for Vaccine Research; used at 1:100 with 5% BSA + 1x PBS) and a dye that stains neuronal Nissl bodies (647-conjugated Neurotrace; Invitrogen, catalog #N21843; used at 1:100 with 5% BSA + 1x PBS), were incubated for 1 hour at 4°C. Fluorescent secondary antibodies that target the primary antibody

24

host species (Donkey anti-Sheep IgG H&L Alexa Fluor 488, Abcam, catalog #ab150177, used at 1:500 with 5% BSA + 1x PBS; Cy™3 AffiniPure Donkey Anti-Rabbit IgG (H+L), Jackson ImmunoResearch, catalog #711-165-152, used at 1:1000 with 5% BSA + 1x PBS) were incubated for 1 hour at RT in order to tag primary antibodies. Hoescht (Bis-benzamide) was incubated for 1 minute to counterstain the nuclei at 450 nanometers (nm). Samples were mounted using a glycerol and polyvinyl alcohol (PVA) mixture.

3.5.3 Congenital model chromogen *in situ* hybridization

Placental tissue samples from six pregnant dams were included in the staining and imaging set; two uninfected control dams and two lethally infected dams; there were no placentas from sublethally infected animals because they are eaten after birth. Liver, uterus, and ovary samples from six pregnant animals were included; two uninfected animals, two sublethally infected animals, and two lethally infected animals. Slides were deparaffinized using an alcohol dehydration series (100%, 95%, and 70%; each step was repeated two times using fresh reagents and a 10-minute incubation time). For colorimetric RNA *in situ* hybridization (ISH), slides underwent an antigen retrieval process by boiling in RNAscope target retrieval reagent for 15 minutes to probe-binding epitopes; slides were placed in a plastic slide holder and submerged in a container of the target retrieval reagent which was microwaved on high power until boiling was achieved then boiling was maintained at a lower power. Slides were stained in slide boxes lined with wet paper towels (in order to create a humidity chamber to prevent the samples from drying out) and placed in an incubator at 37°C in place of the RNAscope hybridization oven; this method was able fit more slides in one experimental run than the hybridization oven, which only holds 20 slides. A primary delete slide, for each tissue type, was incubated with an RNA probe, dapB (a

gene from the soil bacterium, Bacillus subtilis, strain, SMY) that is not found in rat tissues, rather than the RVFV probe; this internal control helps determine if tissues have experienced RNA degradation that would result in non-specific staining. The RNAscope kit instructions state that results are optimal for tissues less than 3 months of age. The RNAscope kit was, otherwise, used according to manufacturer's instructions; RVFV probe incubation for two hours at 37°C, amplifying steps 1-4 for 15-30 minutes at 37°C, and amplifying steps 5-6 for 15 and 30 minutes, respectively, at RT. Enough reagent in each step was pipetted onto the slide to cover the entire tissue. After the staining procedure, slides were dehydrated by air-drying overnight at RT then incubating in xylenes (ethanol was avoided due to RNAscope chromogen, Fast Red, being sensitive and, potentially degraded by alcohols) for 1 minute before mounting with a toluene-based solution, Permount (Fisher Chemical, SP15-100) for long term chromogen staining storage.

3.6 Microscopy and Image Analysis

Immunofluorescent RNA ISH slides were imaged using the Nikon A1 confocal microscope provided by the University of Pittsburgh, Center for Biologic Imaging. Images were contrasted using Adobe Photoshop and denoised and analyzed using Nikon Elements. Images were analyzed for number of specific cell types using Nikon Elements general analysis software. Colorimetric RNA ISH slides were imaged using the Tissue Gnostics pathology microscope provided by the Center for Biologic Imaging. Images were analyzed for total area (μm^2) of infected tissue.

4.0 Results

4.1 Aim 1: To Characterize the Trajectory of RVFV Infection and Corresponding Inflammatory Immune Response in the Nasal Epithelium and Brain During RVF Encephalitis in Lewis Rats.

Rift Valley fever virus (RVFV) is found in the brains of infected rats 1 dpi after subcutaneous (SUBQ) and aerosol (AERO) exposure routes (85, 88); however, aerosol infection carries a higher risk of mortality. The mechanisms behind different disease outcomes due to exposure route is not well understood and this information is crucial for the development of vaccines and therapeutics. Viral antigen and RNA detection quantification methods such as plaque assay, q-RT-PCR, and flow cytometry require homogenization of entire tissues and, while they provide invaluable quantitative data, they lack the ability to show specific events in the trajectory of the virus from the point of exposure. Immunostaining and RNA *in situ* hybridization (ISH) techniques developed in this study highlight RVFV as it travels from the nasal epithelium into the CNS. These methods can be used to elucidate the precise route in which the virus travels to the brain after aerosol exposure. Use of both anti-RVFV NP antibodies and vRNA probes allow for tracking of NP antigen and vRNA, the host cells that are being infected, and the pathway the virus takes from beginning to end-stage disease. We sought to develop a reproducible viral staining method in Lewis rat tissues in order to visualize RVFV infection of the central nervous system (CNS).

Immunofluorescence (IF) staining of RVFV has been achieved in cell culture (88, 97) but staining in tissues yields inconsistent results. Antibodies have been approved for other mediums

such as western blots, ELISAs, and flow cytometry, but many have yet to yield reproducible data for IF and immunohistochemistry (IHC). Optimization of previously developed staining protocols (provided by the University of Pittsburgh Center for Biologic Imaging; adapted from Coons et al. (1941) (98)) and the addition of new steps were required to successfully target RVFV in fixed, frozen Lewis rat CNS tissues. Fixation for complete inactivation of RVFV is required for samples to be removed from BSL-3 conditions; this process requires the rats to be perfused with 4% PFA after euthanasia and for brain tissues to be submerged in fresh 4% PFA for 3 hours before removal. This experiment consisted of fourteen rats (12 infected with RVFV and 2 uninfected controls). Two rats per day (from 1 to 7 dpi) were euthanized. Neuronal death and encephalitis are the main characteristics of neurological RVF, therefore, a staining panel including a neuronal Nissl body marker (Neurotrace), microglial cell marker (IBA-1), and RVFV viral RNA (vRNA) NP probe was carried out on olfactory bulb (OB) and cortex tissues (Fig. 1 and 2) (88). Extracellular vRNA was detected in the glomerular layer (GL) of the OB at 1 dpi and persisted until 3 dpi when the first infected neuron (highlighted by magenta arrow in Fig. 1B) was seen within the GL (yellow masked cells signifying the colocalization of red pseudo-colored vRNA and green neuronal dye). At 4 dpi through end-stage infection, both extracellular and neuronal vRNA staining significantly increased (Fig. 3A). Many neurons lining the mitral cell layer (MCL) colocalized with vRNA by 5 dpi, suggesting that the virus traveled posteriorly from the GL. Virus was found throughout the entirety of the OB and the by 6-7 dpi; nearly 25% of neurons were infected (Fig. 3A). At this time, signal colocalization of vRNA (red), neuronal Nissl bodies (green), and IBA-1 (white) was observed (highlighted by cyan arrow in Fig. 1B) and suggested that activated microglia phagocytosed necrotic neuronal debris. Total microglia (defined at IBA$^+$ cells) increased by more than double the total cell composition of the uninfected sample at 2 dpi and remained elevated for

28

the duration of infection. Microglia at 2 dpi exhibited a ramified structure like that of quiescent microglia but took on a large, amoeboid morphology at 3 dpi until the end of infection (7 dpi); which suggested microglial activation in response to pathogen invasion. These data aligned and largely supported the flow cytometry data in Albe et al. (2019) (88).
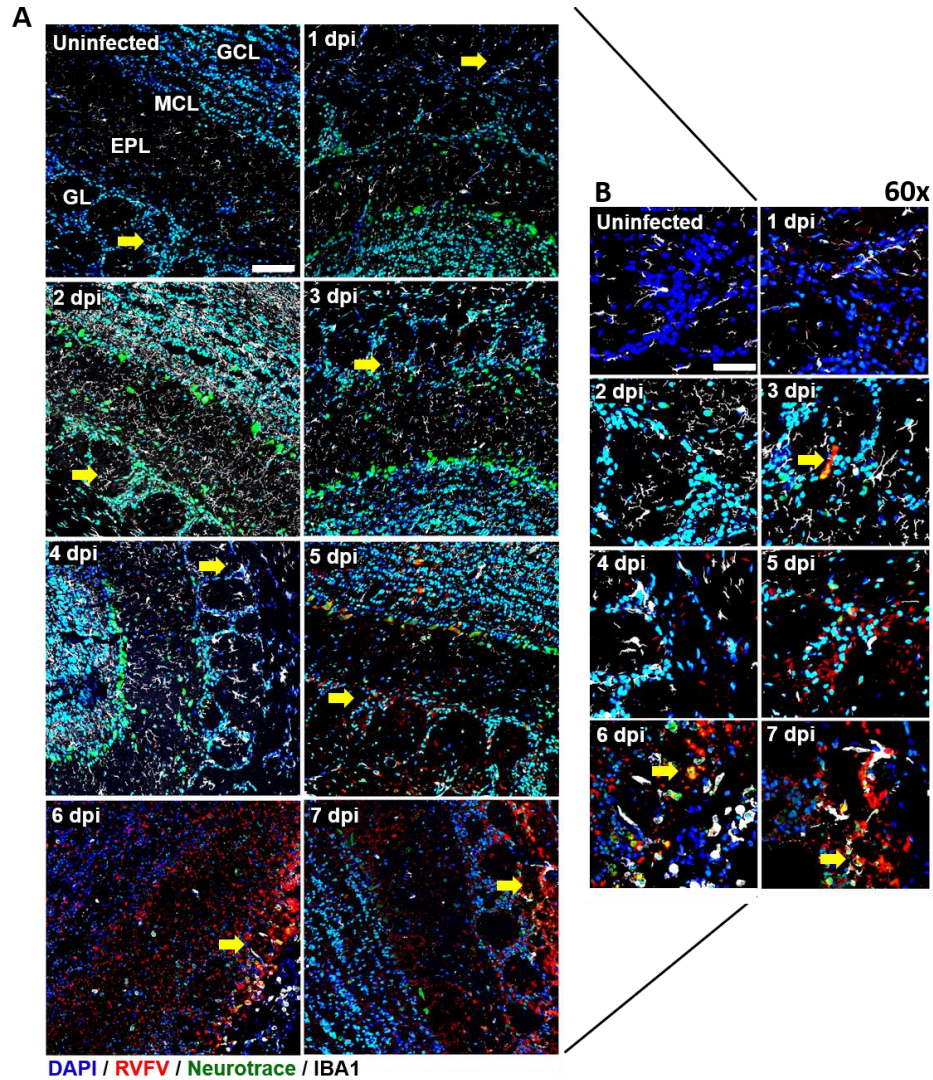
Figure 1: Extracellular RVFV vRNA is seen in the olfactory bulb as early as 1 dpi and neuronal infection occurs at 3 dpi.

Aerosol-infected Lewis rat OBs show evidence of increased viral burden (vRNA) within the glomerular layer from 1 dpi to 7 dpi. RVFV RNA was detected by in situ hybridization immunofluorescence (ISH-IF) (red). Samples were co-stained with an antibody for microglia (IBA-1; white), a Nissl body dye (Neurotrace; green), and a nuclear counterstain (DAPI; blue). (A) 40x micrograph of uninfected control labeled: GL; glomerular layer, EPL; external plexiform layer, MCL; mitral cell layer, GCL; granule cell layer. 2x2 field large images at 40x magnification were stitched using Nikon Elements software (scale bar = 100um). Yellow arrows indicate areas with viral RNA in the glomerular layer that is magnified in (B). (B) Max intensity projection images of the glomerular layer taken at 60x (scale bar = 50um). Yellow arrows indicate infected neurons. (88)

Timing of cellular events in the cortex was similar to that of the OB. Extracellular virus was seen at 1 dpi, but infected neurons were not seen until 3 dpi. Massive neuronal infection and death with phagocytosis of infected neuronal debris by microglia was seen from 5 dpi to 7 dpi. The microglial population spiked at 2 dpi and, over the time course of infection, changed from quiescent, branched structures to activated, macrophage-like morphology. By 7 dpi, the population of infected cells and infected neurons significantly increased to 20% and 30%, respectively (Fig. 3B).
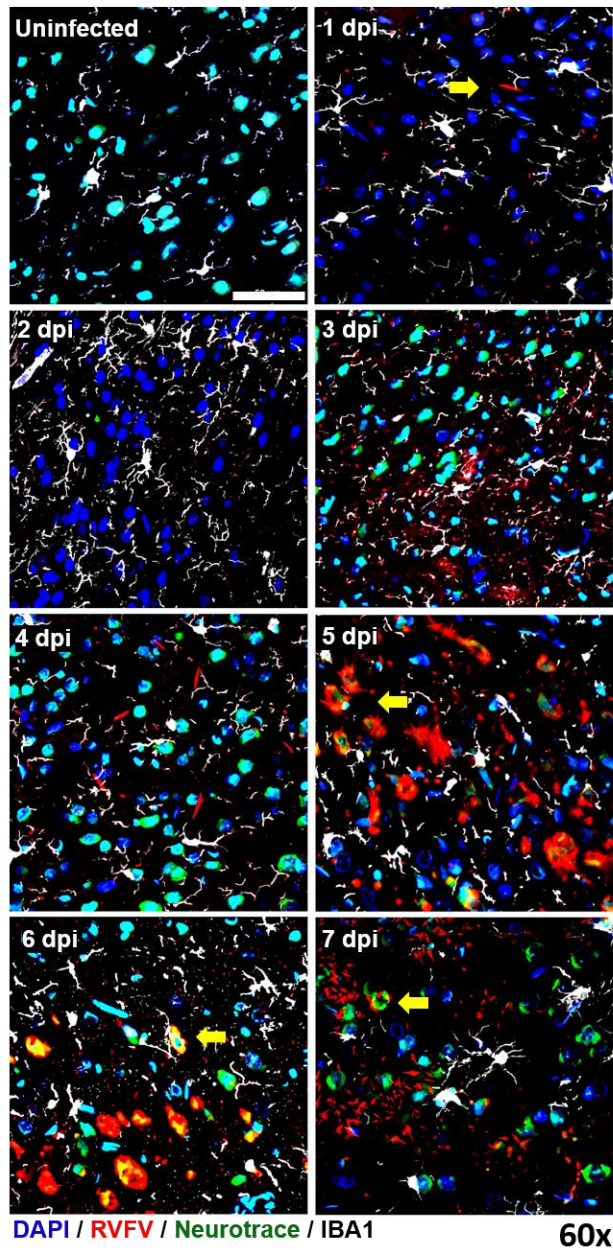
Figure 2: Extracellular RVFV vRNA is seen in the cortex as early as 1 dpi and neuronal infection occurs at 3 dpi.

Aerosol-infected Lewis rat prefrontal cortexes show evidence of increased RVFV vRNA over the course of infection (1 dpi to 7 dpi). RVFV RNA was detected by ISH-IF (red). Samples were co-stained with an antibody for microglia (IBA-1; white), a Nissl body dye (Neurotrace; green), and a nuclear counterstain (DAPI; blue). Yellow arrows highlight infected neurons. Single field 60x magnification images taken with a Nikon A1 confocal microscope (scale bar = 50um).(88)

Flow data in Albe et al. (2019) showed neutrophils and macrophages (peripheral or activated microglia; stained for CD45, a pan leukocyte marker) infiltrating the CNS upon RVFV infection. It is hypothesized that these cells contributed to inflammation and neuronal death. To characterize these cell types, another staining panel (Fig. 4 and 5) was performed using primary antibodies for CD45, myeloperoxidase (MPO) (an antimicrobial enzyme secreted by neutrophils), and IBA-1. The CD45 antibody for IF only detects CD45^{med} to CD45^{high}, which was found in peripheral macrophages and activated microglia; the flow cytometry antibody can detect CD45^{low} expressed by quiescent microglia. However, even with this difference in antibody affinities, the data between the two mediums supported each other. It should be noted that by this IF panel, quiescent vs. activated microglia were mainly distinguished by having branched or amoeboid morphologies whereas peripheral macrophages only exhibited amoeboid morphology.

Leukocytes (green) were seen infiltrating the OB from the BBB to the GL by 1 dpi. These numbers remained low until 5 dpi when a shift in cell composition occurred; neutrophils were seen infiltrating while the number of quiescent microglia decreased and began shifting to the amoeboid shape. At 6 dpi, there was massive breakdown of the BBB and significant, systemic influx of leukocytes (peripheral or activated microglia; CD45$^+$ and IBA$^+$ cells (Fig. 6A-D)) and neutrophils; cells with colocalization of multiple markers also significantly increased on days 6 and 7 dpi (Fig. 6B and 6D). At 7 dpi total cell numbers decreased (Fig. 6B) and localized mainly to the GL. The cortex followed a similar trend aside from showing neutrophil influx at 1 dpi at low numbers which persisted until the BBB breakdown event seen in 5 dpi (Fig. 5). Interestingly, there were branched microglia in the cortex until 7 dpi whereas the microglia population in the olfactory bulb were entirely amoeboid by 5 dpi.

Taken together, these results corroborated data from Albe et al. (2019) showing infiltrating neutrophils and macrophages as a hallmark of encephalitic RVF in Lewis rats. These leukocytes were seen entering the CNS tissues between 2-4 dpi (after initial virus entry at 1 dpi) by complete blood count (CBC) and flow cytometry, then, following the major BBB breakdown event around 5 dpi, infiltrated en masse shortly before mortality. Aerosol exposure consists of inhalation of RVFV droplets through the nose; olfactory epithelial neurons (OEN) within the nasal epithelium connect directly to the OB through the cribriform plate. Due to RVFV initially appearing in the GL of the OB at 1dpi, it seems likely that access to this OENs after aerosol exposure could be the mechanism of severe infection. If RVFV is able to either infect or travel along the OENs between exposure and 1 dpi, then that mechanism could account for the differences in disease outcome between the AERO and SUBQ models. To determine this, nasal epithelium was stained for RVFV-NP antigen, and OEN marker (OMP), and Neurotrace (Fig. 7). On 1 dpi, RVFV antigen was seen along the OEN epithelium and within the lamina propria layer beneath the epithelium. Colocalization of RVFV, OMP, and DAPI (yellow cells) on 1 dpi represented infected nasal epithelial neurons. RVFV signal was at its highest on 3-4 dpi right before the clinical window of disease when neuronal infection began in the OB and cortex. On 5-7 dpi RVFV antigen signal decreased (Fig. 7).

In summary of Aim 1, I have developed a reproducible optimized staining panel to detect both RVFV RNA and NP antigen to identify neuronal infection and inflammatory cell infiltration in Lewis rat nasal epithelium and brain tissues that can be utilized to determine location of these infection events alongside quantitative cell sorting methods used on tissue homogenates.

A **Infected Cell Composition of RVFV Infected Olfactory Bulb**
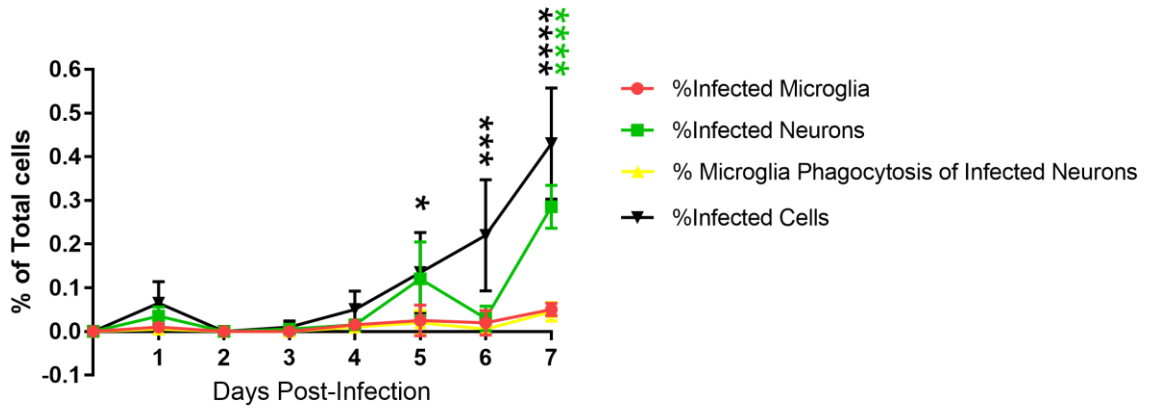
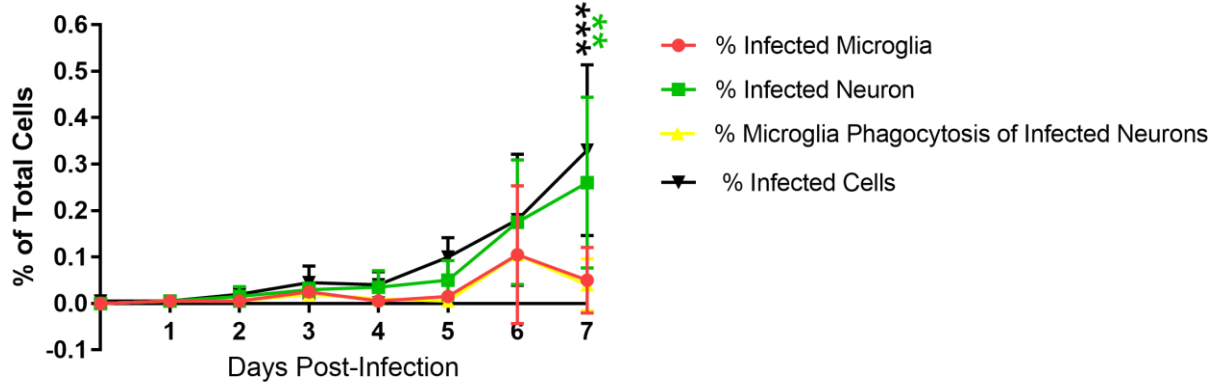**B** **Infected Cell Composition of RVFV Infected Cortex**

Figure 3: Aerosolized RVFV infection results in a significant increase in infected cells during the clinical window.

Mean percentage of infected cell types in the (A) olfactory bulb and (B) cortex over the course of AERO RVFV infection. Two-way ANOVA with multiple comparisons was used to determine statistical significance between daily timepoints and the uninfected control. Infected cell composition was significant in the 5, 6, and 7 dpi samples compared to the uninfected control; infected neuron composition was significant in the 7 dpi samples compared to the infected control (*, $P < 0.05$; **, $P < 0.01$; ***, $P < 0.001$; ****, $P < 0.0001$).
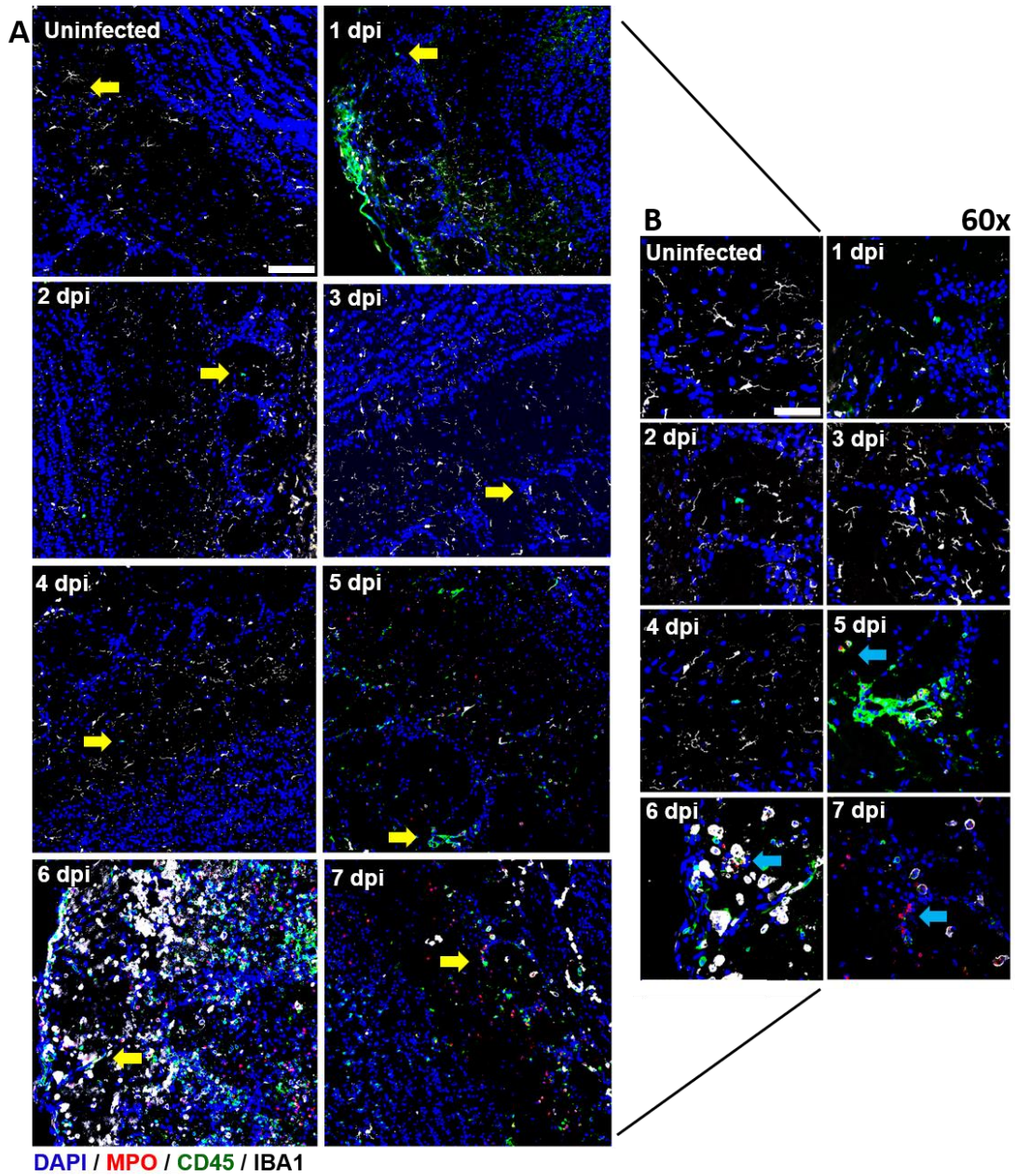
Figure 4: RVFV AERO infection results in leukocyte infiltration into the OB as early as 1 dpi.

Aerosol-infected Lewis rat olfactory bulbs show evidence of increased cell infiltration from 1 dpi to 7 dpi. Samples were stained with primary antibodies to detect neutrophils (MPO; red), a pan-leukocyte marker (CD45; green), and microglia (IBA-1; white) along with a nuclear counterstain (DAPI; blue). (A) 2x2 field images were taken with at 40x magnification (scale bar = 100um). Yellow arrows indicate areas of leukocyte infiltration magnified in (B). (B Max intensity projection images of the olfactory bulb taken at 60x (scale bar = 50um). Cyan arrows indicate neutrophil infiltration. (88)
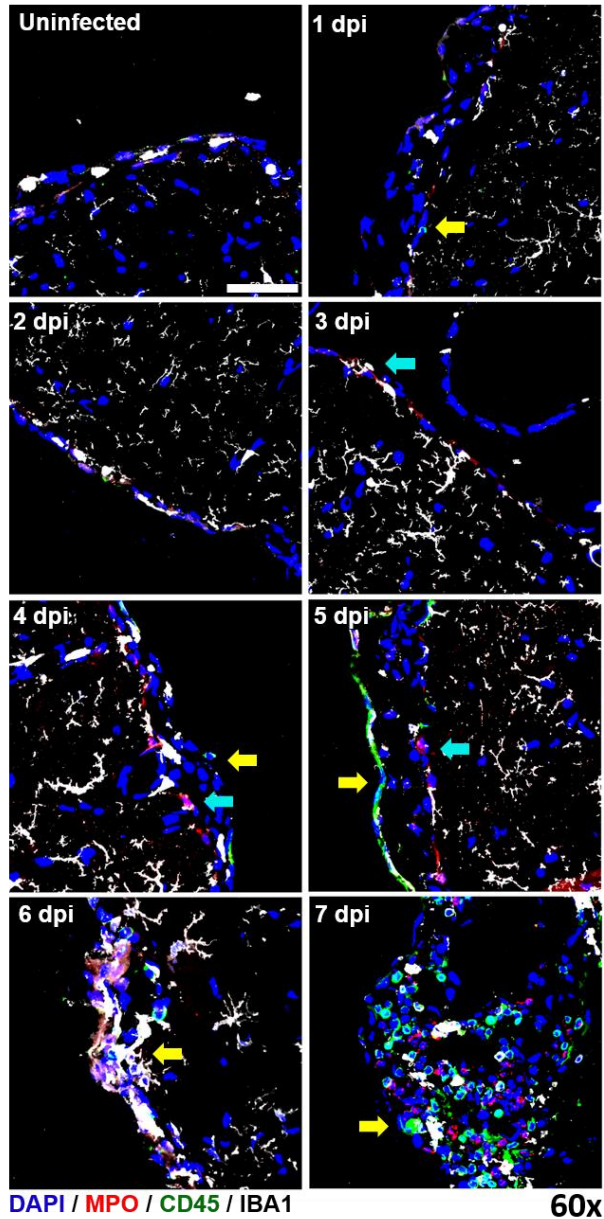
Figure 5: RVFV AERO infection results in leukocyte infiltration into the cortex as early as 1 dpi.

RVFV-infected Lewis rat cortexes show evidence of increased leukocyte cell infiltration from 1 dpi to 7 dpi. Samples were stained with primary antibodies to detect neutrophils (MPO; red), general leukocytes (CD45; green), and microglia (IBA-1; white) along with nuclear counterstain (DAPI; blue). Max intensity projection images of the cortex blood brain barrier taken at 60x. Yellow arrows highlight leukocyte infiltration and cyan arrowheads highlight neutrophil infiltration (Scale bar = 50um). (88)
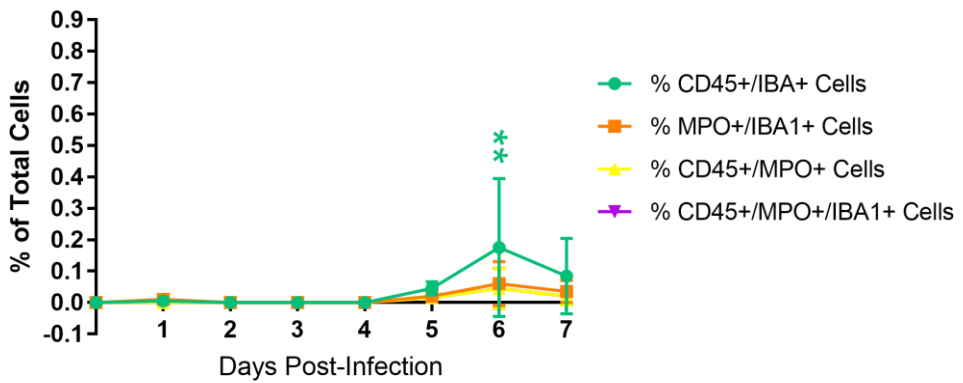
A

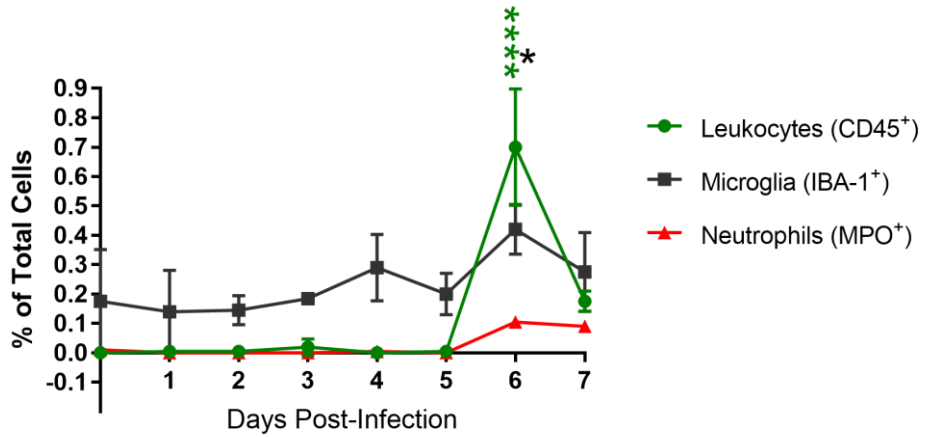**Inflammatory Cell Composition of RVFV-Infected Olfactory Bulb**

B
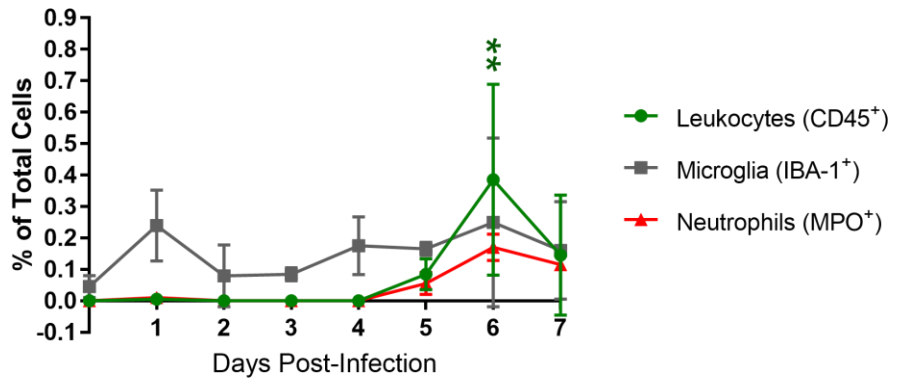
Colocolized Inflammatory Cell Composition of Olfactory Bulb

C

Inflammatory Cell Composition of RVFV-Infected Cortex

D

Colocolized Inflammatory Cell Composition of Cortex
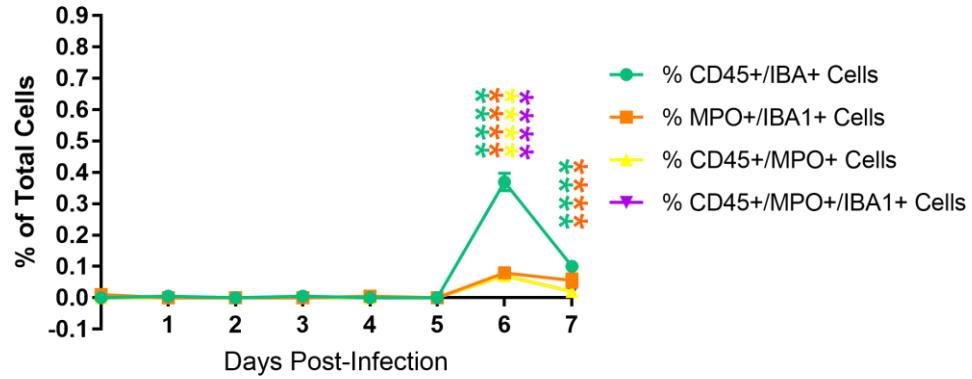
Figure 6: The clinical window of RVF is marked by significant increases in inflammatory immune cells.

Mean percentage of inflammatory cell types in the (A and B) olfactory bulb and (C and D) cortex over the course of AERO RVFV infection. Two-way ANOVA with multiple comparisons was used to determine statistical significance between daily timepoints and the uninfected control. Leukocyte compositions in the olfactory bulb (OB) and cortex were significant in the 6 dpi samples compared to the uninfected control; CD45^{+} microglia compositions in the OB and cortex were significant at 6-7 dpi; MPO^{+} microglial cells, CD45^{+} neutrophils, and MPO^{+} microglia were significant in the cortex at 6-7 dpi compared to the control (*, $P < 0.05$; **, $P < 0.01$; ***, $P < 0.001$; ****, $P < 0.0001$).
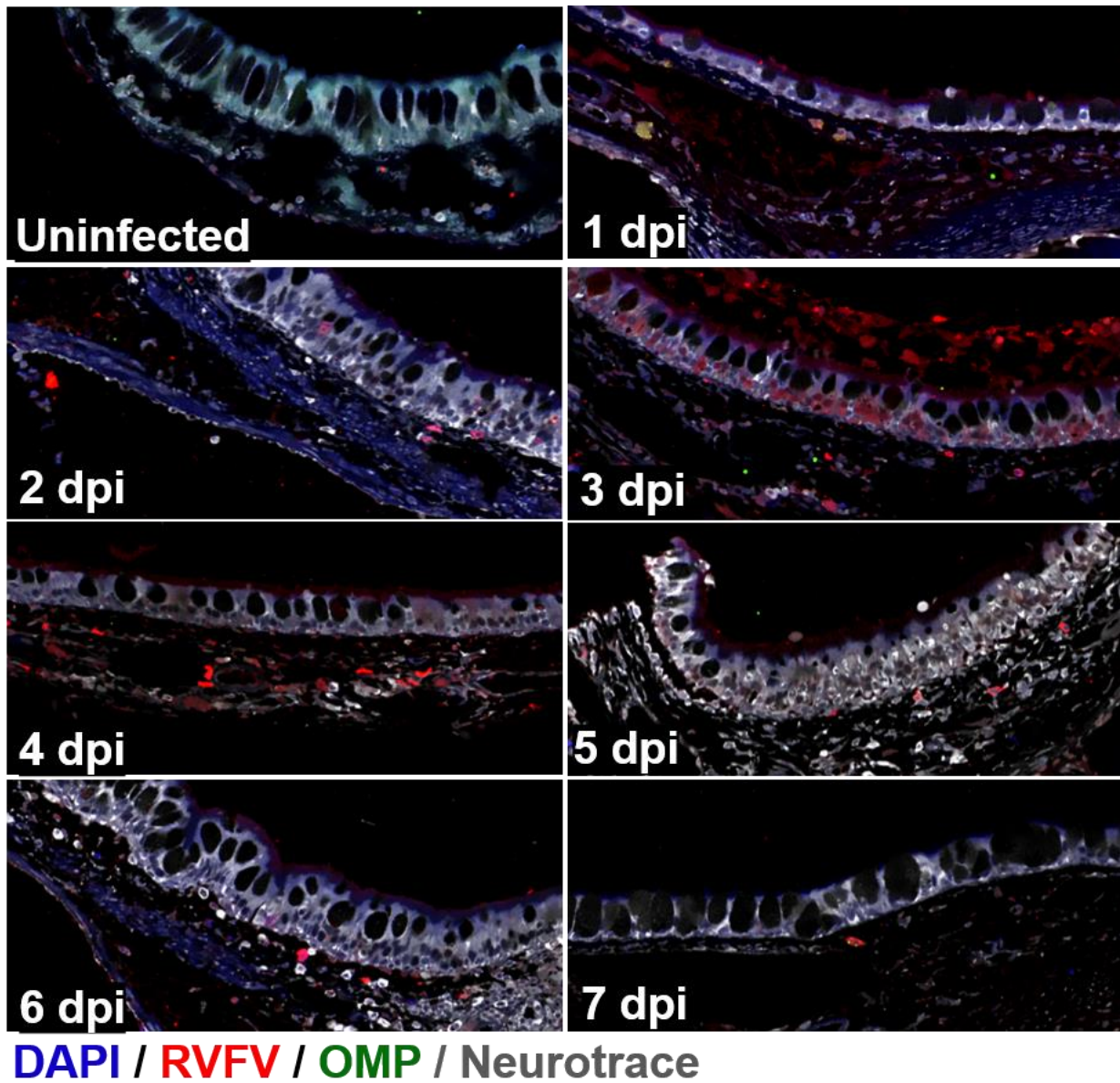
Figure 7: RVFV antigen and infected olfactory epithelial neurons can be seen in the olfactory epithelium and lamina propria as early as 1 dpi.

Images (40x) of aerosol-infected Lewis rat nasal epithelium show evidence of increased RVFV antigen beginning at 1 dpi. RVFV was detected by an anti-NP antibody (red). Samples were co-stained with an antibody for neurons (Neurotrace; white), olfactory epithelial neurons (OMP; green), and a nuclear counterstain (DAPI; blue).

4.2   Aim 2: Define the Mechanism of RVFV Infection and Inflammatory Immune Response in the Placenta of Late-Gestation Pregnant Sprague-Dawley Rats.

Vertical transmission of RVFV has been reported in a handful of human case studies that resulted in neonatal viremia (42), liver pathology (41), and death (42). The ability of RVFV to cause abortion storms in livestock, taken with human cases, suggest that the virus is able to pass to the fetus from an infected mother. The congenital side effects of ZIKV were generally unknown before the outbreak in the Americas in 2015. Of the 28,000 confirmed cases, about 1,000 (4%) were pregnant women (99). The medical consequences of ZIKV illuminated the need for therapeutics for sensitive populations, such as pregnant individuals. *In vivo* experiments by Platt et al. (2018) showed that the encephalitic arboviruses, CHIKV, Powassan virus (POWV), WNV, and Mayaro virus (MAYV) were all able to infect mouse placentas and that WNV and POWV induced fetal demise. In McMillen et al. (2018), our lab was concerned about the ability of RVFV to cross the maternal-fetal interface; therefore, we inoculated pregnant (gestational age E14) SD rats with pathogenic RVFV (ZH501) and examined the maternal and fetal tissues for viral dissemination, cellular targets of infection, and resulting pathology (44).

Typical RVFV IHC techniques showed varying results in rat tissues; the most successful RVFV antibody (IBT Bio Services, Cat# 04-0001) has recently been discontinued. Archived pregnant rat tissues were embedded in paraffin blocks to allow for the preservation of structural integrity and convenient long-term storage. Paraffin wax must be removed in order to dye or stain tissues and requires a xylenes and ethanol dehydration series which can further damage viral and cellular epitopes of interest or cause nonspecific binding of chromogens and fluorophores. Sample preparation and staining required optimization in order to achieve a reproducible method viral detection. The choice to adopt the ACD Bio RNAscope 2.5 HD Red Detection kit assay resulted

from continued failure of current primary antibody options. The probe used in this kit targets an RNA sequence within the nucleocapsid protein (NP) which allows for observation the precise location of NP, the most abundant viral component.

Rats were age-matched and time-mated at 6-8 weeks of age. Presence of a copulation plug was used to verify pregnancy and determine gestational time; early (embryonic day 5 (E5)) or late (E14). Rats were infected via SUBQ hindlimb injection at E14 (when the placenta is fully formed). If rats met euthanasia criteria they were sacrificed, otherwise, they were left to give birth on E22 and were left undisturbed for 5 days postdelivery; during this period, rats often eat placentas so samples from surviving rats were not able to be obtained. Samples from dams that were euthanized previous to E22 (8-9 dpi) were considered lethal samples and dams that survived to give birth were considered sublethal samples. Placental samples were divided into late-gestation and early-gestation groups based on death occurring before or after E19-E20 (5-6 dpi). Exploring differences in fetal development and viral titer between the gestational groups helps to determine the role of infection in fetal demise.

RVFV vRNA was detected in the maternal-fetal interface made up of the maternal decidua and fetal basal zone (seen in Fig. 8A, E, F, and G) in a dam that died at the end of the early-gestation range, on 6 dpi (E20) and in a dam that died late in gestation, while giving birth, at 9 dpi (E23). RVFV is able to infect the same structures between these gestational groups, however, maternal and fetal demise typically occurs in late gestation (44). The additional viral infiltration and resulting massive tissue death within the late gestation placenta may account for the skew towards later mortality. The maternal and fetal interface layers are known to exhibit antiviral and antibacterial immune responses, such as type III IFN production, which renders these tissues resistant to infection by other pathogens such as ZIKV (100). In the case of RVFV, direct infection

42

of this layer may account for high viral loads and lethal fetal outcomes. Trophoblast giant cells (TGC) in the basal zone interact with the maternal decidua to facilitate fetal implantation and become "invasive" once the layers have fused completely (91). It can be seen in Fig. 8G that these cells are also infected by RVFV which suggests another mechanism of direct infection at the maternal-fetal interface. The amnion (Fig. 8E), connective tissue that encapsulates the fetus and amniotic fluid (92), was also the target of infection as well as trophoblast cells within the fetal labyrinth zone (Fig. 8F).
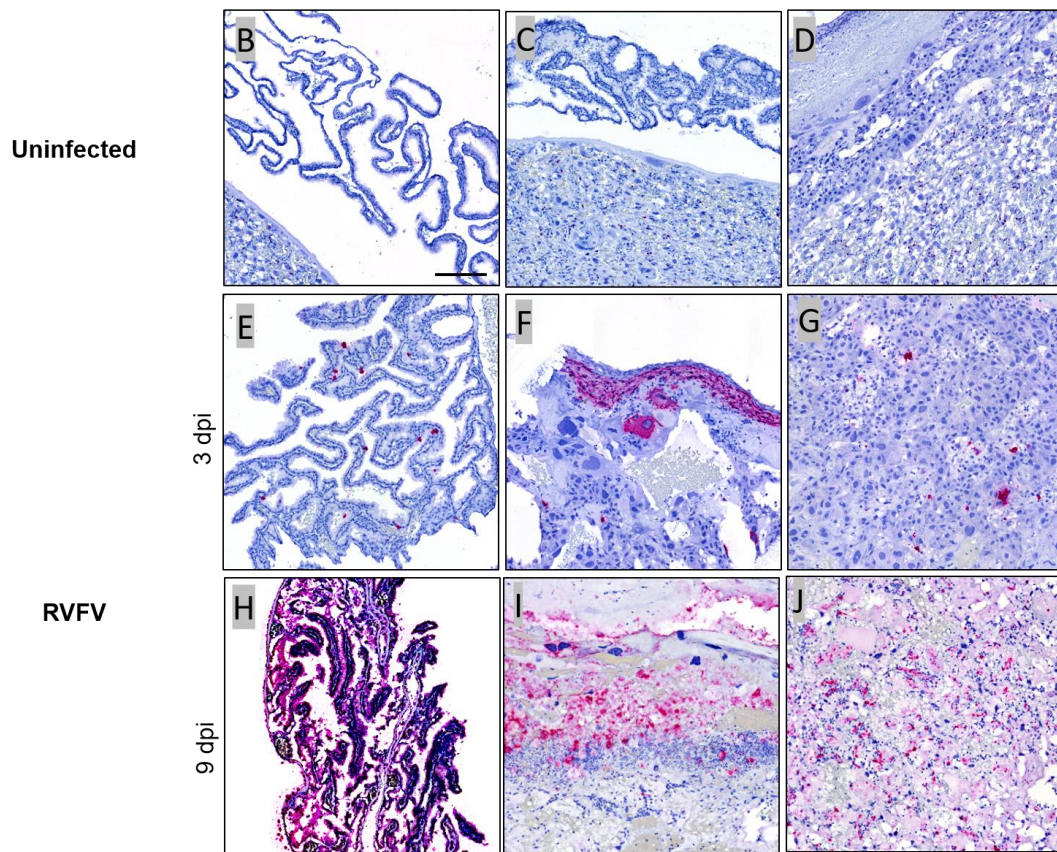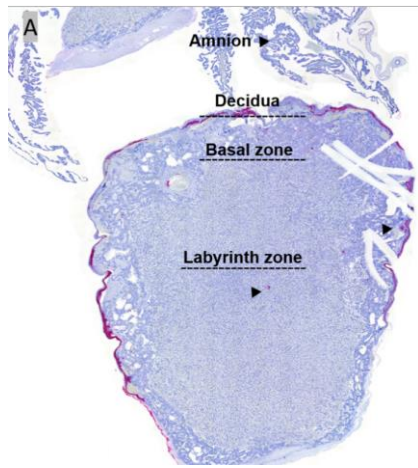
Figure 8: RVFV targets the basal zone, decidua, and amnion of pregnant rat placentas.

Colorimetric RNA ISH staining of RVFV RNA (red) with hematoxylin counterstain (blue). (A) 20x image of infected rat placenta that died 3 dpi/ E20 labeled for relevant maternal and fetal layers (Scale = 250um). (B-D) Uninfected control, (E-G) dam that died 3 dpi, (H-J) dam that died while birthing on 9 dpi. Black arrowheads highlight areas targeted by virus; (B, E, H) amnion, (C, F, I) decidua and trophoblast giant cells of the basal zone, and (D, G, J) trophoblasts within the labyrinth zone (Scale = 25um)**.**

RVFV is considered a promiscuous virus due to its vast tissue tropism. It was originally understood to be a hepatotropic virus, however, depending on the route and model of infection viral loads have been found to be just as high in other organs such as the brain (88) and placenta (44). In congenital RVFV, the uterus and ovaries are targeted by the virus in both lethal and sublethal groups, exhibiting near 10^5 pfu/ml (compared to 10^6 pfu/mL seen in the liver and placenta). Using the liver from lethally infected dams as a positive control tissue for comparison, it can be appreciated that the ovary of the lethally infected pregnant dam in Fig. 9 shows widespread infection. The uterus, to a lesser extent, showed virus throughout, slightly homing to the vasculature edges. Histopathological assessment in McMillen et al. (2018) marked necrotic legions and acute inflammation in the uteruses of both dams lethally and sublethally infected. The ovaries showed no signs of pathology, yet viral RNA was widespread throughout.

McMillen et al. (2018) observed the liver having the second highest amount of viral RNA by qRT-PCR and plaque assay, however, colorimetric ISH analysis showed the liver to have the second lowest amount of viral staining area among the tissues (Fig. 10). Sensitivities in vRNA detection among the techniques may account for these differences. Additional samples of each tissue type must be added to the sample set to increase the reliability of image analysis.

In summary of Aim 2, I have developed a reproducible and optimized staining panel to detect vRNA in FFPE rat tissues in order to determine the cellular targets of RVFV in the placenta and reproductive organs of pregnant rodent model. This model of infection has not yet been studied before its development in McMillen et al. (2018) and will elucidate the effects of ongoing RVFV infection in pregnant rodents as well as animals with similar placental structures.
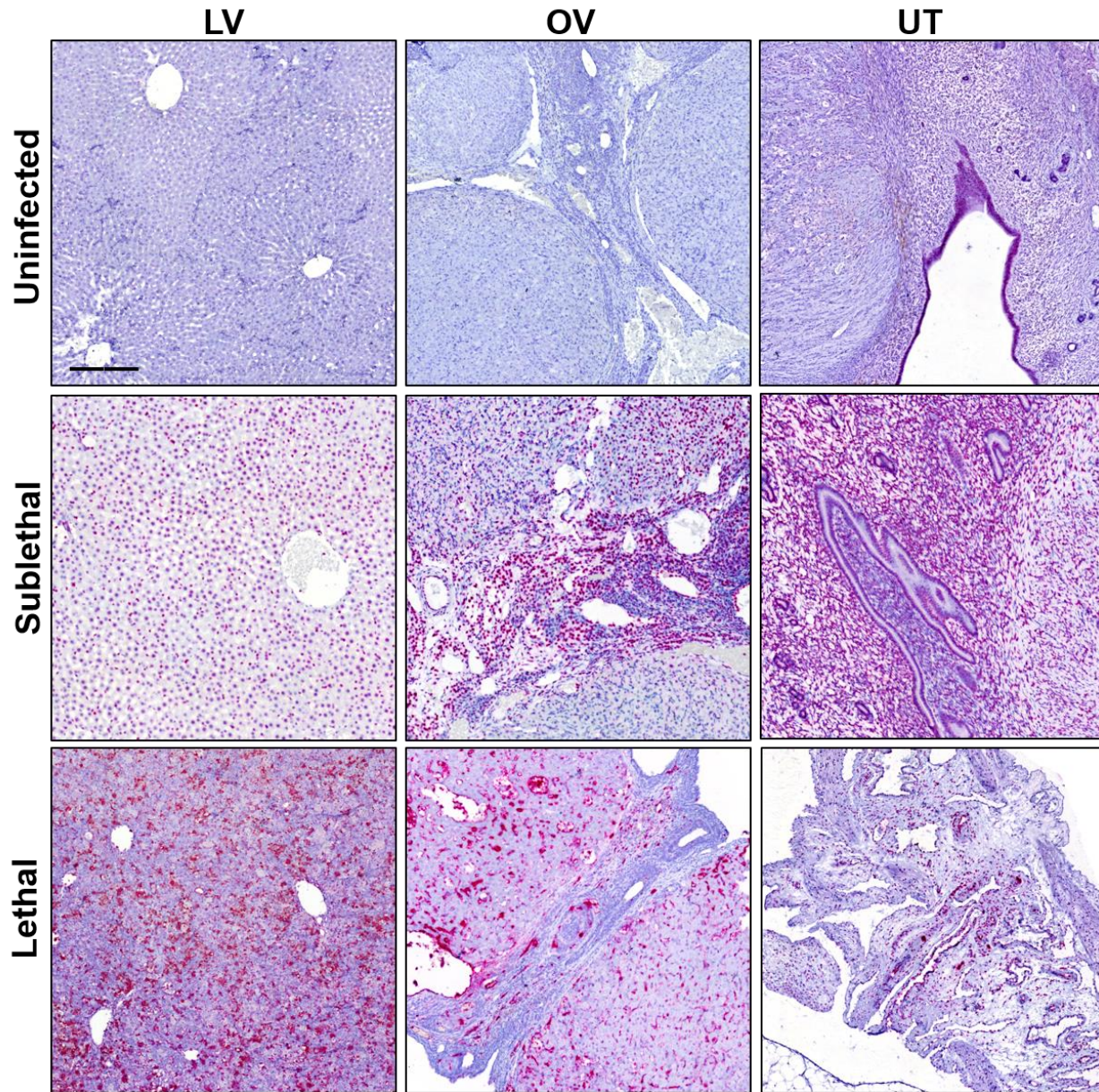
Figure 9: RVFV systemically infects liver, ovaries, and uterus of lethally infected pregnant dam.

Images (20x) of colorimetric RNA ISH staining of RVFV RNA (red) with hematoxylin counterstain (blue) within

the indicated tissues of uninfected, lethally infected, and sublethally infected dams. (Scale bar = 100um).
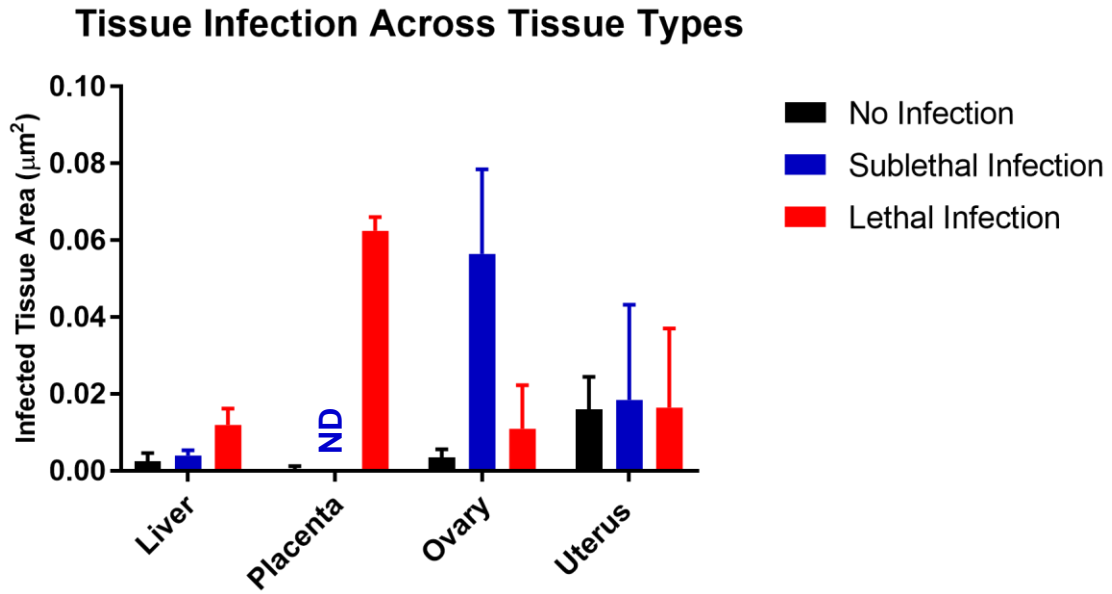
Figure 10: The reproductive organs of infected dams exhibit more vRNA staining than the liver during congenital RVFV infection.

Colorimetric ISH images from uninfected, sublethally infected, and lethally infected pregnant dam tissues were measured for vRNA area (μm^2) and normalized against total tissue area (μm^2). Placentas from sublethally infected dams were not available for analysis; only uninfected and lethally infected are represented.

5.0 Discussion

Since its official discovery in 1931 (12), Rift Valley fever virus (RVFV) has caused known outbreaks in continental Africa (12, 13, 15-19, 101), the Saudi Peninsula (8), Madagascar (20), and Yemen (8). Massive livestock mortality events highlight the economic burden of RVFV epidemics. While mosquitos facilitate subcutaneous (SUBQ) disease spread between livestock, wild ruminants, and humans, exposure to aerosolized (AERO) RVFV from inhalation of infected tissues and feces may be associated with a higher risk of severe disease outcomes such as meningoencephalitis (85, 88) or ocular disease (8, 39, 40). Human cases of respiratory exposure to RVFV have occurred in laboratory settings but have not been reported from outbreaks during endemic regions; there is not enough epidemiological data to link exposure with severe disease outcomes. Aerosol infection studies in rats (56, 82, 85-88), mice (77-79), and non-human primates (NHPs) (93, 94) have shown higher mortality rates than other exposure routes such as SUBQ (88) and intraperitoneal (IP) (102). RVFV has been aerosolized by the United States (US) and Russian governments and remains highly stable and able to be transmitted via inhalation (73) and can be used as a potential bioterrorism agent (54, 103).

A large case study of 683 individuals with laboratory confirmed (IgM$^+$) Rift Valley fever (RVF) during the Saudi outbreak characterized the most common symptoms as fever (93%), central nervous system (CNS) manifestations (17%), hemorrhagic manifestations (7%), and vision loss (2%) (8). Of the 81 individuals with CNS symptoms, confusion, lethargy, disorientation, vertigo, coma, tremors, and amnesia all made up more than 1% of cases. Individuals with CNS symptoms were also 14.2 times more likely to succumb to disease than those without a neurological component (8); this is the highest odds ratio behind bleeding manifestations resulting

in a 20 times higher likelihood of death. One case of an RVFV-seropositive individual in South Africa in 1975 dying of meningo-encephalitis showed pathological signs of perivascular cuffing and round-cell infiltration (104) which are also seen in the brains of NHP models exposed to aerosolized RVF (93). The development of NHP and rodent models of encephalitic RVF are crucial research tools for illuminating the mechanism of infection separating self-limiting febrile disease from severe CNS and ocular outcomes.

Albe et al. (2019) compared the mortality and clinical manifestations of Lewis rat models exposed to AERO and SUBQ RVFV; AERO rats developed neurological symptoms (decreased activity, hunched posture, porphyrin staining of the eyes and nose, erratic behavior, circling, or rolling (82)) by 5 dpi and succumbed to disease between 6-7 dpi whereas SUBQ rats survived and never developed clinical symptoms. The most striking finding between the two exposure models was that viral RNA was found in the brains of both models at 1 dpi (88). The ability to fight off CNS infection in the SUBQ model vs. the AERO model is not understood and is a critical piece of the puzzle for therapeutic options targeting neurological RVF. The data generated in Albe et al. (2019) via q-rt-PCR, complete blood count (CBC), and flow cytometry quantified viral titer and cell composition from whole tissue homogenates, whereas AIM 1 in this paper sought to determine this information from 7μm thick tissue sections in order to highlight specific areas of viral and immune cell infiltration to better hone in on the mechanism of infection.

IF microscopy results corroborated the event of major viral RNA increase in the olfactory bulb happening between 4-5 dpi, with the percentage of infected cells increasing up to 40% in the olfactory bulb (OB) and 30% in the cortex There is a small increase of infected cells, infected microglia and infected neurons in the OB on 1 dpi; this trend occurs on 2 dpi in the cortex. The viral staining panel also allowed visualization of viral descent into the OB of rats, originating in

the GL as early as 1 dpi and infecting neurons by 3 dpi. The glomerular layer (GL) contains the axons of olfactory epithelial neurons (OEN) which are the point of attachment between the CNS component of the snout and the OB; the initial presence of RVFV in this region suggests the ability of the virus to either directly infect OENs and enter the brain (as seen with herpes simplex type-1 virus (105)) or travel through neuron unsheathing cell channels (as seen in LACV infection (106)) rather than other mechanisms such as hematogenous entry via interruption of the blood brain barrier (BBB) (as seen with Ebstein-Barr virus (107)) "trojan horse" entry into the BBB via infection of monocytes (as seen in SIV infection (108)), or travel through neuromuscular junctions (as seen with poliovirus (109, 110)). Viral RNA (vRNA) is not seen near the endothelial outer layer of the BBB in the immunofluorescence (IF) micrographs during early infection which should, otherwise, be observed if it were the initial infection route. A staining panel with CD45 and RVFV would be necessary to judge whether the trojan horse method of entry is occurring, although, there are not infected cells near the BBB perimeter in either the OB or cortex.

RVFV antigen is seen within the OEN and lamina propria layer of nasal epithelium at 1 dpi which supports the idea that AERO exposure may allow for extensive viral entry into the OB by these mechanisms which can overwhelm the immune response; virus entering the brain at 1 dpi in the SUBQ model may not yield a high enough amount of infectious virus, which could account for the differences in disease severity. Additional research into the role of OENs during RVFV AERO infection will be necessary to determine the exact mechanism of CNS entry and to target for therapeutics for neurological disease. Entire RVFV-infected rat heads with intact OBs would be necessary for viral and axonal staining to observe whether the virus is infecting OENs or traveling through ensheathing channels. Munster V.J. et al. (2012) shows immunohistochemistry (IHC) micrographs of Nipah virus antigen colocalizing with OEN axons crossing the cribriform

plate in hamster nasal epithelium (111); developing similar staining panels would help determine RVFV's entry mechanism.

Confirmed cases of human vertical transmission of RVFV are limited to two case studies resulting in two infected pregnant women giving birth to both an infant with jaundice, an enlarged liver, and an enlarged spleen (41), and an IgM$^+$ infant that died a week after delivery (42), respectively, and a cross-sectional study that found that 54% of pregnant women (15 of 28) with an ongoing RVFV infection experienced a late-term miscarriage (odds ratio 7·4, 95% CI 2·7–20·1; p<0·0001) (43). While epidemiological data on this occurrence in humans is limited, the prevalence of abortion storms among livestock suggests that the virus is able to target reproductive tissues and pass to fetuses. McMillen et al. (2018) developed a reproducible rodent model of congenital RVF to address vertical transmission in a model that more similarly represents the placental structure of humans.

Human and rat placentas are hemochorial, meaning the maternal blood is in direct contact with the chorion, the outermost membrane that encloses the embryo (92) and forms a maternal-fetal interface. They are also both discoid-shaped, meaning there is a single placenta formed that has a discus structure (112). These similarities allow for rats to be used as models of placental and reproductive toxicology that can be loosely extrapolated to humans, however, there are key differences in the structures that need to be noted. The maternal-fetal interface of the rat is made up of three layers (trichorial) of syncytiotrophoblast cells, whereas the human placenta only has one layer (monochorial; this begins as two separate that fuse in the first trimester (113)) made up of syncytiotrophoblasts and cytotrophoblasts (112). Within the interface, on the fetal side, the labyrinth zone of rats is functionally similar to the villous layer of humans; humans have more extreme extravillous trophoblast invasion of the interface than rats (113). The middle layer, the

basal zone of rats is similarly to the basal plate of humans. The maternal-most layer, the decidua and metrial gland are similar to the decidua of humans (112); the metrial gland contains endometrial stromal cells, arteries, fibroblasts, and uterine natural killer cells (uNK). The yolk sac of the rat placenta eventually grows to cover the amnion and embryo and contributes nutrients, whereas the human yolk stalk becomes vestigial after the first trimester (112). Developmental issues of the yolk sac in the rats can lead to fetal malformations (113) which adds other concerns for infection mechanism differences between the models. The layer separating the yolk sac from the embryo in the fetal membrane, the amnion, is found in both human and rodents; the absence of the yolk sac in humans may allow more virus to pass to the amnion which has shown to be permissive to RVFV infection. These differences, taken together, highlight the importance of recognizing structural dissimilarities and the roles they may play during infection and transmission.

RVFV vRNA is observed within each of the three layers of the rat placenta; the decidua and metrial gland, basal zone, and labyrinth zone, yolk sac, and amnion. Platt et al. (2018) performed footpad injection of flaviviruses (Powassan virus (POWV) and West Nile Virus (WNV) and alphaviruses (Chikungunya virus (CHIKV) and Mayaro virus (MAYV)) on pregnant, wildtype (WT) mice and found that all viruses were able to infect and replicate in the placenta, however, only POWV and WNV caused fetal demise. Further investigation showed WNV and POWV vRNA in each of the three layers by RNA ISH and qtPCR, however, CHIKV and MAYV did not replicate efficiently in the villi and decidual layers (100). The alphavirus infectivity is similar to that seen in ZIKV infection of WT mice (114). The inability of other viruses capable of congenital infection to successfully infect the maternal decidua and fetal labyrinth zones of rodent highlights the unique tropism of RVFV. Syncytiotrophoblast cells within the labyrinth zone and fetal-

52

maternal interface are typically resistant to viral infections due to production of type III interferons (114), such as interferon-γ (IFNγ), which can induce T-cell activation and differentiation and MHC class II expression (78). However, the NSs of bunyaviruses acts as an interferon antagonist, suggesting an ability to avoid the immune protections of certain placental layers.

Human second-trimester placental explant experiments support the ability of RVFV (44) , POWV, WNV, and ZIKV (100) to infect similar structures (the decidua and villi) whereas CHIKV cannot replicate efficiently in the decidua or villi. Despite differences in rodent and human placental structure, RVFV, and potentially, other bunyaviruses, have the ability to circumvent antiviral immune responses in rodent and human placentas. This must be further investigated using cell-specific markers for IHC/IF to determine specific targets within these layers.

McMillen et al (2018) observed viral replication in the ovaries and uterus of lethal and sublethal pregnant dams. Severe pathology including liquefactive necrosis of the uterus was observed (44), which is unusual considering the pregnant uterus is thought to be immune-privileged and can downregulate immune responses to avoid tissue damage in response to neonatal antigen (115). This suggests that either RVFV alone has the ability to cause severe uterine pathology or that maternal immune cells such as uNK cells become active in response to infection. Further immune cell-specific and inflammatory cytokine staining needs to be carried out to illuminate the mechanism of tissue damage during congenital RVF.

Rodent models of neurological and congenital RVF allow for observation into the unique tropisms of RVFV. Structural similarities between the CNS and reproductive systems of rodents and humans illuminate the potential of RVFV infection to cause multiple, severe disease outcomes in its endemic countries as well as naive populations in the event of its spread to new countries. The aims in this thesis are a preliminary observation into the poorly understudied disease

manifestations of RVF and serve to open the door for mechanistic studies to uncover new

mitigation strategies and potential therapeutics.

Bibliography

1. Gaudreault NN, Indran SV, Balaraman V, Wilson WC, Richt JA. Molecular aspects of Rift Valley fever virus and the emergence of reassortants. Virus Genes. 2019;55(1):1-11.

2. Bird BH, Ksiazek TG, Nichol ST, Maclachlan NJ. Rift Valley fever virus. J Am Vet Med Assoc. 2009;234(7):883-93.

3. Turell MJ, Presley SM, Gad AM, Cope SE, Dohm DJ, Morrill JC, et al. Vector competence of Egyptian mosquitoes for Rift Valley fever virus. Am J Trop Med Hyg. 1996;54(2):136-9.

4. Reisen WK, Fang Y, Martinez VM. Effects of temperature on the transmission of west nile virus by Culex tarsalis (Diptera: Culicidae). J Med Entomol. 2006;43(2):309-17.

5. Turell MJ, Linthicum KJ, Patrican LA, Davies FG, Kairo A, Bailey CL. Vector competence of selected African mosquito (Diptera: Culicidae) species for Rift Valley fever virus. J Med Entomol. 2008;45(1):102-8.

6. Turell MJ, Britch SC, Aldridge RL, Kline DL, Boohene C, Linthicum KJ. Potential for mosquitoes (Diptera: Culicidae) from Florida to transmit Rift Valley fever virus. J Med Entomol. 2013;50(5):1111-7.

7. F. Glyn Davies VM. Recognizing Rift Valley Fever. Rome: Food And Agriculture Organization Of The United Nations; 2003.

8. Madani TA, Al-Mazrou YY, Al-Jeffri MH, Mishkhas AA, Al-Rabeah AM, Turkistani AM, et al. Rift Valley fever epidemic in Saudi Arabia: epidemiological, clinical, and laboratory characteristics. Clin Infect Dis. 2003;37(8):1084-92.

9. CDC. Federal Select Agent Program, Select Agents and Toxins 2017 [Available from: https://www.selectagents.gov/SelectAgentsandToxins.html.

10. Nash D, Mostashari F, Fine A, Miller J, O'Leary D, Murray K, et al. The outbreak of West Nile virus infection in the New York City area in 1999. N Engl J Med. 2001;344(24):1807-14.

11. Daubney RaJH. Rift valley fever. East Afr Med J. 1933;10:2-19.

12. Daubney RaJH. Enzootic hepatitis or Rift Valley Fever: an undescribed virus disease of sheep, cattle, and man from east Africa. Journak of Pathology and Bacteriology 1931;34:545-79.

13. Murithi RM, Munyua P, Ithondeka PM, Macharia JM, Hightower A, Luman ET, et al. Rift Valley fever in Kenya: history of epizootics and identification of vulnerable districts. Epidemiol Infect. 2011;139(3):372-80.

14. Organization WH. Rift Valley fever: World Health Organization; 2018 [Available from: https://www.who.int/news-room/fact-sheets/detail/rift-valley-fever.

15. Laughlin LW, Meegan JM, Strausbaugh LJ, Morens DM, Watten RH. Epidemic Rift Valley fever in Egypt: observations of the spectrum of human illness. Trans R Soc Trop Med Hyg. 1979;73(6):630-3.

16. Hassan OA, Ahlm C, Sang R, Evander M. The 2007 Rift Valley fever outbreak in Sudan. PLoS Negl Trop Dis. 2011;5(9):e1229.

17. Swai ES, Sindato C. Seroprevalence of Rift Valley fever virus infection in camels (dromedaries) in northern Tanzania. Trop Anim Health Prod. 2015;47(2):347-52.

18. Sow A, Faye O, Ba Y, Diallo D, Fall G, Faye O, et al. Widespread Rift Valley Fever Emergence in Senegal in 2013-2014. Open Forum Infect Dis. 2016;3(3):ofw149.

19. Caminade C, Ndione JA, Diallo M, MacLeod DA, Faye O, Ba Y, et al. Rift Valley Fever outbreaks in Mauritania and related environmental conditions. Int J Environ Res Public Health. 2014;11(1):903-18.

20. Lancelot R, Beral M, Rakotoharinome VM, Andriamandimby SF, Heraud JM, Coste C, et al. Drivers of Rift Valley fever epidemics in Madagascar. Proc Natl Acad Sci U S A. 2017;114(5):938-43.

21. Gaudreault NN, Indran SV, Bryant PK, Richt JA, Wilson WC. Comparison of Rift Valley fever virus replication in North American livestock and wildlife cell lines. Front Microbiol. 2015;6:664.

22. Evans A, Gakuya F, Paweska JT, Rostal M, Akoolo L, Van Vuren PJ, et al. Prevalence of antibodies against Rift Valley fever virus in Kenyan wildlife. Epidemiol Infect. 2008;136(9):1261-9.

23. Capobianco Dondona A, Aschenborn O, Pinoni C, Di Gialleonardo L, Maseke A, Bortone G, et al. Rift Valley Fever Virus among Wild Ruminants, Etosha National Park, Namibia, 2011. Emerg Infect Dis. 2016;22(1):128-30.

24. Youssef BZ. The potential role of pigs in the enzootic cycle of rift valley Fever at alexandria governorate, egyp. J Egypt Public Health Assoc. 2009;84(3-4):331-44.

25. Neitzel DF, Grimstad PR. Serological Evidence Of California Group And Cache Valley Virus Infection In Minnesota White-Tailed Deer. Journal of Wildlife Diseases. 1991;27(2):230-7.

26. Wilson WC, Kim IJ, Trujillo JD, Sunwoo SY, Noronha LE, Urbaniak K, et al. Susceptibility of White-Tailed Deer to Rift Valley Fever Virus. Emerg Infect Dis. 2018;24(9):1717-9.

27. Smithburn KC. Rift Valley fever; the neurotropic adaptation of the virus and the experimental use of this modified virus as a vaccine. Br J Exp Pathol. 1949;30(1):1-16.

28. Francis T, Magill TP. Immunological Studies With The Virus Of Influenza. J Exp Med. 1935;62(4):505-16.

29. de Boer SM, Kortekaas J, de Haan CA, Rottier PJ, Moormann RJ, Bosch BJ. Heparan sulfate facilitates Rift Valley fever virus entry into the cell. J Virol. 2012;86(24):13767-71.

30. Harmon B, Schudel BR, Maar D, Kozina C, Ikegami T, Tseng CT, et al. Rift Valley fever virus strain MP-12 enters mammalian host cells via caveola-mediated endocytosis. J Virol. 2012;86(23):12954-70.

31. Lozach PY, Kuhbacher A, Meier R, Mancini R, Bitto D, Bouloy M, et al. DC-SIGN as a receptor for phleboviruses. Cell Host Microbe. 2011;10(1):75-88.

32. Fields BN, David M. Knipe, Peter M. Howley. Fields Virology. 5 ed. Philadelphia Wolters Kluwer Health/Lippincott Williams & Wilkins 2007.

33. Won S, Ikegami T, Peters CJ, Makino S. NSm protein of Rift Valley fever virus suppresses virus-induced apoptosis. J Virol. 2007;81(24):13335-45.

34. Terasaki K, Won S, Makino S. The C-terminal region of Rift Valley fever virus NSm protein targets the protein to the mitochondrial outer membrane and exerts antiapoptotic function. J Virol. 2013;87(1):676-82.

35. Colon-Ramos DA, Irusta PM, Gan EC, Olson MR, Song J, Morimoto RI, et al. Inhibition of translation and induction of apoptosis by Bunyaviral nonstructural proteins bearing sequence similarity to reaper. Mol Biol Cell. 2003;14(10):4162-72.

36. Le May N, Dubaele S, Proietti De Santis L, Billecocq A, Bouloy M, Egly JM. TFIIH transcription factor, a target for the Rift Valley hemorrhagic fever virus. Cell. 2004;116(4):541-50.

37. Van Velden DJ, Meyer JD, Olivier J, Gear JH, McIntosh B. Rift Valley fever affecting humans in South Africa: a clinicopathological study. S Afr Med J. 1977;51(24):867-71.

38. GM F. The virus of rift valley fever or enzootic hepatitis Lancet. 1931(221):1350-1.

39. Strausbaugh LJ, Laughlin LW, Meegan JM, Watten RH. Clinical studies on Rift Valley fever, Part I: Acute febrile and hemorrhagic-like diseases. J Egypt Public Health Assoc. 1978;53(3-4):181-2.

40. Centers for Disease Control and Prevention, Division of High-Consequence Pathogens and Pathology (DHCPP), Viral Special Pathogens Branch (VSPB). Rift Valley fever (RVF) 2016 [updated October 19, 2016. Available from: https://www.cdc.gov/vhf/rvf/index.html.

41. Adam I, Karsany MS. Case report: Rift Valley Fever with vertical transmission in a pregnant Sudanese woman. J Med Virol. 2008;80(5):929.

42. Arishi HM, Aqeel AY, Al Hazmi MM. Vertical transmission of fatal Rift Valley fever in a newborn. Ann Trop Paediatr. 2006;26(3):251-3.

43. Baudin M, Jumaa AM, Jomma HJE, Karsany MS, Bucht G, Naslund J, et al. Association of Rift Valley fever virus infection with miscarriage in Sudanese women: a cross-sectional study. Lancet Glob Health. 2016;4(11):e864-e71.

44. McMillen CM, Arora N, Boyles DA, Albe JR, Kujawa MR, Bonadio JF, et al. Rift Valley fever virus induces fetal demise in Sprague-Dawley rats through direct placental infection. Sci Adv. 2018;4(12):eaau9812.

45. Arora N, Sadovsky Y, Dermody TS, Coyne CB. Microbial Vertical Transmission during Human Pregnancy. Cell Host Microbe. 2017;21(5):561-7.

46. Ikegami T, Balogh A, Nishiyama S, Lokugamage N, Saito TB, Morrill JC, et al. Distinct virulence of Rift Valley fever phlebovirus strains from different genetic lineages in a mouse model. PLoS One. 2017;12(12):e0189250.

47. Indran SV, Ikegami T. Novel approaches to develop Rift Valley fever vaccines. Front Cell Infect Microbiol. 2012;2:131.

48. Von Teichman B, Engelbrecht A, Zulu G, Dungu B, Pardini A, Bouloy M. Safety and efficacy of Rift Valley fever Smithburn and Clone 13 vaccines in calves. Vaccine. 2011;29(34):5771-7.

49. Faburay B, Wilson WC, Gaudreault NN, Davis AS, Shivanna V, Bawa B, et al. A Recombinant Rift Valley Fever Virus Glycoprotein Subunit Vaccine Confers Full Protection against Rift Valley Fever Challenge in Sheep. Sci Rep. 2016;6:27719.

50. Brown JL, J.W. Dominik, and E.W. Larson. Airborne Survival of Rift Valley Fever Virus DTIC USAMRIID. 1982.

51. Christopher GW, Cieslak TJ, Pavlin JA, Eitzen EM, Jr. Biological warfare. A historical perspective. Jama. 1997;278(5):412-7.

52. Ermler ME, Yerukhim E, Schriewer J, Schattgen S, Traylor Z, Wespiser AR, et al. RNA Helicase Signaling Is Critical for Type I Interferon Production and Protection against Rift Valley Fever Virus during Mucosal Challenge. Journal of Virology. 2013;87(9):4846-60.

53. Ikegami T, Hill TE, Smith JK, Zhang L, Juelich TL, Gong B, et al. Rift Valley Fever Virus MP-12 Vaccine Is Fully Attenuated by a Combination of Partial Attenuations in the S, M, and L Segments. J Virol. 2015;89(14):7262-76.

54. Borio L, Inglesby T, Peters CJ, Schmaljohn AL, Hughes JM, Jahrling PB, et al. Hemorrhagic fever viruses as biological weapons: medical and public health management. Jama. 2002;287(18):2391-405.

55. Gould EA, Higgs S. Impact of climate change and other factors on emerging arbovirus diseases. Trans R Soc Trop Med Hyg. 2009;103(2):109-21.

56. Bales JM, Powell DS, Bethel LM, Reed DS, Hartman AL. Choice of inbred rat strain impacts lethality and disease course after respiratory infection with Rift Valley Fever Virus. Front Cell Infect Microbiol. 2012;2:105.

57. Kilgore PE, Ksiazek TG, Rollin PE, Mills JN, Villagra MR, Montenegro MJ, et al. Treatment of Bolivian hemorrhagic fever with intravenous ribavirin. Clin Infect Dis. 1997;24(4):718-22.

58. McCormick JB, King IJ, Webb PA, Scribner CL, Craven RB, Johnson KM, et al. Lassa fever. Effective therapy with ribavirin. N Engl J Med. 1986;314(1):20-6.

59. Scharton D, Bailey KW, Vest Z, Westover JB, Kumaki Y, Van Wettere A, et al. Favipiravir (T-705) protects against peracute Rift Valley fever virus infection and reduces delayed-onset neurologic disease observed with ribavirin treatment. Antiviral Res. 2014;104:84-92.

60. Kende M, Lupton HW, Rill WL, Levy HB, Canonico PG. Enhanced therapeutic efficacy of poly(ICLC) and ribavirin combinations against Rift Valley fever virus infection in mice. Antimicrob Agents Chemother. 1987;31(7):986-90.

61. Sidwell RW, J. H. Huffman, B.B. Barnett, and D.Y. Pifat. In vitro and in vivo Phlebovirus inhibition by ribavirin. Antimicrob Agents Chemother. 1988(32):331-6.

62. Reed C, Lin K, Wilhelmsen C, Friedrich B, Nalca A, Keeney A, et al. Aerosol exposure to Rift Valley fever virus causes earlier and more severe neuropathology in the murine model, which has important implications for therapeutic development. PLoS Negl Trop Dis. 2013;7(4):e2156.

63. Enria DA, Briggiler, A.M., S. Levis, Vallejos, D., Maiztegui, J.I., and Canonico, P.G. . Tolerance and antiviral effect of ribavarin in patients with Argentine hemorrhagic fever. Antiviral Res. 1987(7):353-9.

64. Gowen BB, Wong MH, Jung KH, Sanders AB, Mendenhall M, Bailey KW, et al. In vitro and in vivo activities of T-705 against arenavirus and bunyavirus infections. Antimicrob Agents Chemother. 2007;51(9):3168-76.

65. Gowen BB, Wong MH, Jung KH, Smee DF, Morrey JD, Furuta Y. Efficacy of favipiravir (T-705) and T-1106 pyrazine derivatives in phlebovirus disease models. Antiviral Res. 2010;86(2):121-7.

66. Hawman DW, Haddock E, Meade-White K, Williamson B, Hanley PW, Rosenke K, et al. Favipiravir (T-705) but not ribavirin is effective against two distinct strains of Crimean-Congo hemorrhagic fever virus in mice. Antiviral Res. 2018;157:18-26.

67. Tani H, Komeno T, Fukuma A, Fukushi S, Taniguchi S, Shimojima M, et al. Therapeutic effects of favipiravir against severe fever with thrombocytopenia syndrome virus infection in a lethal mouse model: Dose-efficacy studies upon oral administration. PLoS One. 2018;13(10):e0206416.

68. Westover JB, Rigas JD, Van Wettere AJ, Li R, Hickerson BT, Jung KH, et al. Heartland virus infection in hamsters deficient in type I interferon signaling: Protracted disease course ameliorated by favipiravir. Virology. 2017;511:175-83.

69. Caroline AL, Powell DS, Bethel LM, Oury TD, Reed DS, Hartman AL. Broad spectrum antiviral activity of favipiravir (T-705): protection from highly lethal inhalational Rift Valley Fever. PLoS Negl Trop Dis. 2014;8(4):e2790.

70. Liu L, Celma CC, Roy P. Rift Valley fever virus structural proteins: expression, characterization and assembly of recombinant proteins. Virol J. 2008;5:82.

71. Naslund J, Lagerqvist N, Habjan M, Lundkvist A, Evander M, Ahlm C, et al. Vaccination with virus-like particles protects mice from lethal infection of Rift Valley Fever Virus. Virology. 2009;385(2):409-15.

72. Dodd KA, Bird BH, Metcalfe MG, Nichol ST, Albarino CG. Single-dose immunization with virus replicon particles confers rapid robust protection against Rift Valley fever virus challenge. J Virol. 2012;86(8):4204-12.

73. Swanepoel R, Struthers JK, Erasmus MJ, Shepherd SP, McGillivray GM, Erasmus BJ, et al. Comparison of techniques for demonstrating antibodies to Rift Valley fever virus. J Hyg (Lond). 1986;97(2):317-29.

74. Heise MT, Whitmore A, Thompson J, Parsons M, Grobbelaar AA, Kemp A, et al. An alphavirus replicon-derived candidate vaccine against Rift Valley fever virus. Epidemiol Infect. 2009;137(9):1309-18.

75. Golnar AJ, Kading RC, Hamer GL. Quantifying the potential pathways and locations of Rift Valley fever virus entry into the United States. Transbound Emerg Dis. 2018;65(1):85-95.

76. Kasari TR, Carr DA, Lynn TV, Weaver JT. Evaluation of pathways for release of Rift Valley fever virus into domestic ruminant livestock, ruminant wildlife, and human populations in the continental United States. J Am Vet Med Assoc. 2008;232(4):514-29.

77. Dodd KA, McElroy AK, Jones TL, Zaki SR, Nichol ST, Spiropoulou CF. Rift valley Fever virus encephalitis is associated with an ineffective systemic immune response and activated T

cell infiltration into the CNS in an immunocompetent mouse model. PLoS Negl Trop Dis. 2014;8(6):e2874.

78. Bouloy M, Janzen C, Vialat P, Khun H, Pavlovic J, Huerre M, et al. Genetic evidence for an interferon-antagonistic function of rift valley fever virus nonstructural protein NSs. J Virol. 2001;75(3):1371-7.

79. Lorenzo G, Martin-Folgar R, Hevia E, Boshra H, Brun A. Protection against lethal Rift Valley fever virus (RVFV) infection in transgenic IFNAR(-/-) mice induced by different DNA vaccination regimens. Vaccine. 2010;28(17):2937-44.

80. Smith DR, Steele KE, Shamblin J, Honko A, Johnson J, Reed C, et al. The pathogenesis of Rift Valley fever virus in the mouse model. Virology. 2010;407(2):256-67.

81. Peters CJ, Slone TW. Inbred rat strains mimic the disparate human response to Rift Valley fever virus infection. J Med Virol. 1982;10(1):45-54.

82. Caroline AL, Kujawa MR, Oury TD, Reed DS, Hartman AL. Inflammatory Biomarkers Associated with Lethal Rift Valley Fever Encephalitis in the Lewis Rat Model. Front Microbiol. 2015;6:1509.

83. Ruzek D, Salat J, Singh SK, Kopecky J. Breakdown of the blood-brain barrier during tick-borne encephalitis in mice is not dependent on CD8+ T-cells. PLoS One. 2011;6(5):e20472.

84. Michlmayr D, McKimmie CS, Pingen M, Haxton B, Mansfield K, Johnson N, et al. Defining the chemokine basis for leukocyte recruitment during viral encephalitis. J Virol. 2014;88(17):9553-67.

85. Walters AW, Kujawa MR, Albe JR, Reed DS, Klimstra WB, Hartman AL. Vascular permeability in the brain is a late pathogenic event during Rift Valley fever virus encephalitis in rats. Virology. 2019;526:173-9.

86. Wang P, Dai J, Bai F, Kong KF, Wong SJ, Montgomery RR, et al. Matrix metalloproteinase 9 facilitates West Nile virus entry into the brain. J Virol. 2008;82(18):8978-85.

87. Winkler CW, Race B, Phillips K, Peterson KE. Capillaries in the olfactory bulb but not the cortex are highly susceptible to virus-induced vascular leak and promote viral neuroinvasion. Acta Neuropathol. 2015;130(2):233-45.

88. Albe JR, Boyles DA, Walters AW, Kujawa MR, McMillen CM, Reed DS, et al. Neutrophil and macrophage influx into the central nervous system are inflammatory components of lethal Rift Valley fever encephalitis in rats. PLoS Pathog. 2019;15(6):e1007833.

89. McElroy AK, Nichol ST. Rift Valley fever virus inhibits a pro-inflammatory response in experimentally infected human monocyte derived macrophages and a pro-inflammatory

cytokine response may be associated with patient survival during natural infection. Virology. 2012;422(1):6-12.

90. Shope RE. Bunyaviruses Medical Microbiology. 4th ed. Galveston, TX: The University of Texas Medical Branch at Galveston.; 1996.

91. Soares MJ, Chakraborty D, Karim Rumi MA, Konno T, Renaud SJ. Rat placentation: an experimental model for investigating the hemochorial maternal-fetal interface. Placenta. 2012;33(4):233-43.

92. Furukawa S, Hayashi S, Usuda K, Abe M, Hagio S, Ogawa I. Toxicological pathology in the rat placenta. J Toxicol Pathol. 2011;24(2):95-111.

93. Hartman AL, Powell DS, Bethel LM, Caroline AL, Schmid RJ, Oury T, et al. Aerosolized rift valley fever virus causes fatal encephalitis in african green monkeys and common marmosets. J Virol. 2014;88(4):2235-45.

94. Morrill JC, Jennings GB, Johnson AJ, Cosgriff TM, Gibbs PH, Peters CJ. Pathogenesis of Rift Valley fever in rhesus monkeys: role of interferon response. Arch Virol. 1990;110(3-4):195-212.

95. Anderson GW, Jr., Slone TW, Jr., Peters CJ. The gerbil, Meriones unguiculatus, a model for Rift Valley fever viral encephalitis. Arch Virol. 1988;102(3-4):187-96.

96. Alers JC, Krijtenburg PJ, Vissers KJ, van Dekken H. Effect of bone decalcification procedures on DNA in situ hybridization and comparative genomic hybridization. EDTA is highly preferable to a routinely used acid decalcifier. J Histochem Cytochem. 1999;47(5):703-10.

97. Mroz C, Schmidt KM, Reiche S, Groschup MH, Eiden M. Development of monoclonal antibodies to Rift Valley Fever Virus and their application in antigen detection and indirect immunofluorescence. J Immunol Methods. 2018;460:36-44.

98. Coons AH, Creech HJ, Jones RN. Immunological Properties of an Antibody Containing a Fluorescent Group. Proceedings of the Society for Experimental Biology and Medicine. 1941;47(2):200-2.

99. Centers for Disease Control and Prevention NCfEaZIDN, Division of Vector-Borne Diseases (DVBD). Zika virus CDC; 2019 [updated June 4, 2019. Available from: https://www.cdc.gov/zika/index.html.

100. Platt DJ, Smith AM, Arora N, Diamond MS, Coyne CB, Miner JJ. Zika virus-related neurotropic flaviviruses infect human placental explants and cause fetal demise in mice. Sci Transl Med. 2018;10(426).

101. Gerdes GH. Rift Valley fever. Rev Sci Tech. 2004;23(2):613-23.

102. Le Coupanec A, Babin D, Fiette L, Jouvion G, Ave P, Misse D, et al. Aedes mosquito saliva modulates Rift Valley fever virus pathogenicity. PLoS Negl Trop Dis. 2013;7(6):e2237.

103. Sidwell RW, Smee DF. Viruses of the Bunya- and Togaviridae families: potential as bioterrorism agents and means of control. Antiviral Res. 2003;57(1-2):101-11.

104. McIntosh BM, Russell D, dos Santos I, Gear JH. Rift Valley fever in humans in South Africa. S Afr Med J. 1980;58(20):803-6.

105. Smith GA, Gross SP, Enquist LW. Herpesviruses use bidirectional fast-axonal transport to spread in sensory neurons. Proceedings of the National Academy of Sciences. 2001;98(6):3466-70.

106. Bennett RS, Cress CM, Ward JM, Firestone CY, Murphy BR, Whitehead SS. La Crosse virus infectivity, pathogenesis, and immunogenicity in mice and monkeys. Virol J. 2008;5:25.

107. Casiraghi C, Dorovini-Zis K, Horwitz MS. Epstein-Barr virus infection of human brain microvessel endothelial cells: A novel role in multiple sclerosis. Journal of Neuroimmunology. 2011;230(1):173-7.

108. Clay CC, Rodrigues DS, Ho YS, Fallert BA, Janatpour K, Reinhart TA, et al. Neuroinvasion of fluorescein-positive monocytes in acute simian immunodeficiency virus infection. J Virol. 2007;81(21):12040-8.

109. Crotty S, Hix L, Sigal LJ, Andino R. Poliovirus pathogenesis in a new poliovirus receptor transgenic mouse model: age-dependent paralysis and a mucosal route of infection. Journal of General Virology. 2002;83(7):1707-20.

110. Ohka S, Igarashi H, Nagata N, Sakai M, Koike S, Nochi T, et al. Establishment of a Poliovirus Oral Infection System in Human Poliovirus Receptor-Expressing Transgenic Mice That Are Deficient in Alpha/Beta Interferon Receptor. Journal of Virology. 2007;81(15):7902-12.

111. Munster VJ, Prescott JB, Bushmaker T, Long D, Rosenke R, Thomas T, et al. Rapid Nipah virus entry into the central nervous system of hamsters via the olfactory route. Sci Rep. 2012;2:736.

112. Furukawa S, Tsuji N, Sugiyama A. Morphology and physiology of rat placenta for toxicological evaluation. J Toxicol Pathol. 2019;32(1):1-17.

113. Schmidt A, Morales-Prieto DM, Pastuschek J, Frohlich K, Markert UR. Only humans have human placentas: molecular differences between mice and humans. J Reprod Immunol. 2015;108:65-71.

114. Miner JJ, Cao B, Govero J, Smith AM, Fernandez E, Cabrera OH, et al. Zika Virus Infection during Pregnancy in Mice Causes Placental Damage and Fetal Demise. Cell. 2016;165(5):1081-91.

115.Arck P, Solano ME, Walecki M, Meinhardt A. The immune privilege of testis and gravid uterus: same difference? Mol Cell Endocrinol. 2014;382(1):509-20.